UNIVERSITÄT STUTTGART

BACHELOR'S THESIS

Setup and characterization of an ultra-narrow linewidth laser system at 1001 nm

---

A thesis submitted in partial fulfillment of the requirements for the degree of Bachelor of Science

by

Tim JEGLORTZ

Examiner:
Prof. Dr. Tilman PFAU

Dipolar Quantum Gases Group
5. Physikalisches Institut

September 1, 2023

Declaration of Authorship

Hiermit versichere ich gemäß § 27 Abs. 7 der Prüfungsordnung der Universität Stuttgart für den Bachelorstudiengang Physik vom 31.07.2015,

- dass ich diese Arbeit selbstständig verfasst habe,
- dass ich keine anderen als die angegebenen Quellen verwendet und alle wörtlich oder sinngemäß aus anderen Werken übernommenen Aussagen als solche gekennzeichnet habe,
- dass die eingereichte Arbeit weder vollständig noch in wesentlichen Teilen Gegenstand eines anderen Prüfungsverfahrens gewesen ist und,
- dass das elektronische Exemplar mit den anderen Exemplaren übereinstimmt.

Stuttgart, 01.09.2023 *Tim Jeglortz*

Abstract

This thesis is aiming to characterize the properties of a laser system at 1001 nm with a narrow linewidth that will be used for the addressing of a very narrow transition in dysprosium as part of a quantum gas microscope experiment. A basic optics setup is installed that allows for investigating the relevant specifications. A systematic power monitoring over weeks yielded information about the ability of the involved Tapered Amplifier to provide an output power in the region up to 2 W. The behavior of the wavelength that can be fine-tuned with a frequency resolution of at least 20 MHz will be part of the discussion as well as the analysis of the wavelength drift over hours in case of the locked and the free running laser. The delayed self-heterodyne linewidth measurement method is used to make an estimation of the linewidth leading to a value $< 10\,\mathrm{Hz}$. The ultra-narrow linewith is directly linked to the locking to the ultra-low expansion cavity. Its high finesse around $\mathcal{F} = 410000$ can be verified by the application of an adapted version of the ring-down spectroscopy.

Zusammenfassung

Diese Arbeit befasst sich umfänglich mit der Charakterisierung eines 1001 nm Lasersystems, welches für die Adressierung eines sehr schmalbandigen Übergangs in Dysprosium verwendet werden soll, der Bestandteil des sich im Aufbau befindlichen Quantengasmikroskops sein wird. Ein fundamentaler Optik-Aufbau ist Grundlage für alle weiteren Messungen. Das systematische Überwachen der Laserleistung über einen Zeitraum von Wochen ermöglicht es, Aussagen über die Fähigkeiten des Halbleiterlaserverstärkers, der Leistungen im Bereich bis zu 2 W liefert, zu treffen. Das Verhalten der Wellenlänge, die mit einer Frequenzauflösung von mindestens 20 MHz feinjustiert werden kann, ist Bestandteil der Diskussion, ebenso wie der über Stunden gemessene Drift der Wellenlänge, sowohl im Falles des gelockten als auch des nicht gelockten Lasers. Das Selbst-Heterodyn-Verfahren kann zur Abschätzung der Linienbreite des Lasers auf einen Wert unter 10 Hz verwendet werden. Die sehr gerine Linienbreite steht in direkter Verbindung mit dem Laserresonator. Dessen hohe Finesse kann mit Hilfe des Ring-Down-Verfahrens auf $\mathcal{F} \approx 410000$ bestimmt werden.

Contents

1 Introduction

Lasers have become a fundamental part of almost every experiment in modern atomic physics for a long time. What makes them one of the most versatile tools is the ability to provide nearly perfect coherent and monochromatic light that has a very large field of application. Trapping, cooling, imaging, spectroscopy and much more in the field of ultra-cold quantum gases depends on the reliability of lasers.

Within this thesis a laser system at 1001 nm is characterized that combines two crucial properties: The ultra-narrow linewidth of an external cavity diode laser with the high power gain of a Tapered Amplifier what predestines it for various high-precision applications. The aim is to implement the laser in the future into the upcoming quantum gas microscope experiment with dysprosium atoms. The quantum gas microscope is an amazing tool that enables reaching new fields in many-body quantum systems described by the Hubbard model. It is exemplarily predestined for quantum simulations that allow to explore models where numeric computations hardly manage to get small results. [1, 12]

This work should be a user's guide that gathers all relevant parameters and settings for the problem-free operation of this system for any future demand.

In chapter 2 a short introduction to the properties of dysprosium and the future application of the laser system is given.
In chapter 3 the components of the laser system are presented and some fundamental theoretical principles and experimental techniques that all correspond to the narrow linewidth are briefly introduced.
The chapter 4 contains the characterization of the laser system and forms the core of this thesis. The chapter start with the presentation of the basic optics setup and continues with the description of the single properties. The relevant settings and achievable values for power and wavelength are discussed. Furthermore, the experimental results of the methods to determine the linewidth of the laser and the finesse of the cavity are explained.
Finally, chapter 5 summarizes the extensive explanations and underlines the suitability of this laser system for high-precision experiments.

2 Dysprosium

Several atoms have been in the focus of research groups in the field of ultracold physics over the past few years. In the Ultracold Quantum Gases group at the 5$^{\text{th}}$ Institute of Physics (PI5) at the University of Stuttgart, dysprosium is the atom of choice. The rare-earth element of the lanthanide series with the atomic number $Z = 66$ has seven stable isotopes. The four with the highest abundance are the bosonic ^{162}Dy (25 %) and ^{164}Dy (28 %) as well as the fermionic ^{161}Dy (19 %) and ^{163}Dy (25 %) [3]. Dysprosium is of special interest because with $10\mu_B$ it possesses the largest magnetic moment of the naturally occurring elements [20] leading to strong dipole-dipole interactions. The long-range and anisotropic characteristics have recently led to the discovery of new states of matter in Bose-Einstein condensates as quantum droplets or supersolids [5] that are also part of the research at PI5.

2.1 1001 nm Transition

The extract of the level scheme of dysprosium shown in Figure 2.1 gives an overview of the numerous states and their energy levels. Among the available transitions, recently the 1001 nm transition from the $[\mathrm{Xe}]4\mathrm{f}^{10}6\mathrm{s}^2(^5\mathrm{I}_8)$ ground state to the excited $4\mathrm{f}^9(^6\mathrm{H}^\circ)5\mathrm{d}6\mathrm{s}^2(^7\mathrm{I}^\circ_9)$ [26, 21] state is of particular interest. The excited state was recently characterized to have a lifetime of at least $\tau = 87(7)$ ms corresponding to a linewidth of only $\Gamma/2\pi = 1.8(2)$ Hz [24]. There are some direct applications for this transition like the possibility to use it for further laser-cooling of an atomic gas or to do energy-resolved imaging.

The current plan is to use it in the future experiment to explore the physics of the extended dipolar Hubbard model with either bosons or fermions in a quantum gas microscope. For the creation of a quantum gas microscope, an ultraviolet (UV) optical lattice is used to trap single atoms. By changing the lattice properties, one can control the strength of the nearest-neighbor-interactions. Since the spacing of the optical lattice is smaller than the resolution limit of a normal microscope, a special sub-wavelength imaging technique has to be implemented to reach single-atom resolution. The optical lattice gets modified in a way that every second atoms experiences a slightly different potential. This is the requirement for being able to use the narrow 1001 nm transition to excite only half of the atoms to the long-living so called shelving state. The magic wavelength of 1001 nm ensures that the atoms are always trapped in the UV lattice, independent whether they are in the ground state or in the excited shelving state. In the mean time, the atoms

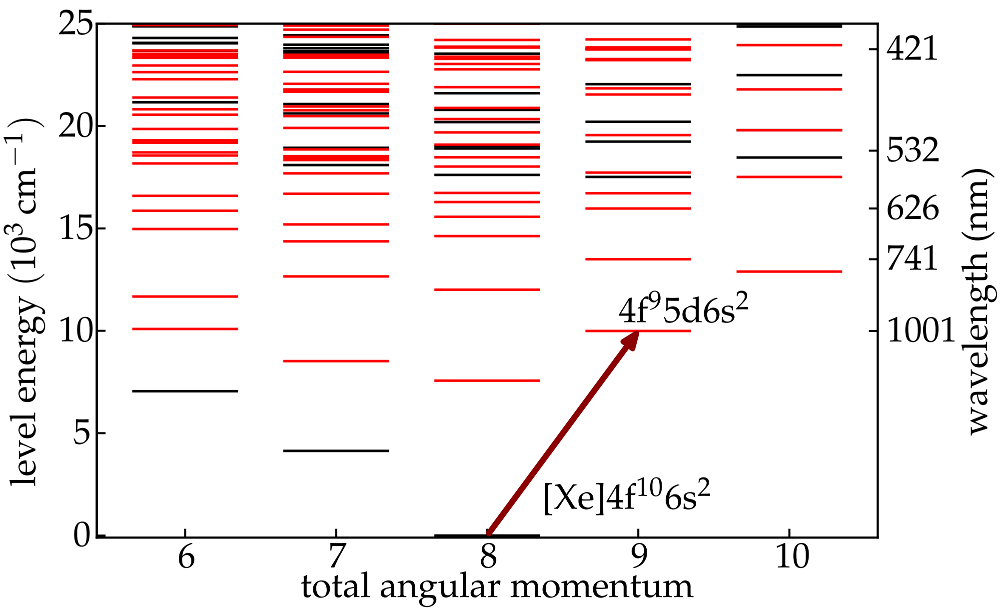

FIGURE 2.1: Extract of the level scheme of dysprosium. Atomic states with even parity are drawn in black, those with odd parity are red. The relevant 1001 nm transition is marked with an arrow and the electron configurations of the involved states are written next to the levels. This transition is very narrow with a linewidth of only 1.8(2) Hz [24]. (figure adapted from [26])

that remain in the ground state can be imaged using the broader 421 nm transition. Afterwards, half of the atoms that were "stored" in the shelving state decay spontaneously back into the ground state and can then be imaged as well. Superimposing both images finally provides a singe-atom resolved image of the initial lattice occupation. For a more detailed description, see reference [26].

This very short introduction shall only give an idea of possible future applications, however they are not part of this thesis.

3 Ultra-narrow Linewidth Laser System

The laser system that is the basis of this thesis consists of multiple components that are combined to ideally create a stable and powerful laser light source with an ultra-narrow linewidth. A few relevant aspects of such a system for the following characterization are discussed within this section.

3.1 The 1001 nm Laser System

In this thesis the *Toptica TA pro* laser system at 1001 nm is going to be characterized. It consists of an external cavity diode laser (ECDL) coupled to an ultra-low expansion (ULE) cavity that provides a feedback-signal for the Pound–Drever–Hall (PDH) locking technique. Since diode lasers usually only reach a power below 1 W, the diode laser seeds a Tapered Amplifier (TA). With the *DLC pro* controller, there is a possibility to control the laser system digitally and obtain further information, e.g about the current system parameters.

Diode lasers can have a very narrow linewidth, but their power might be insufficient for many applications that require a power higher than a few hundred milliwatts. This is the point where Tapered Amplifiers might be a possible solution. They reach higher powers up to a few watts depending on the desired wavelength and provide still a good beam quality without compromising the favorable spectral qualities of the seeding laser. TAs are semiconductor optical amplifiers where the incident light is coupled into a single-mode channel that leads to a special shaped gain region. The beam is confined in one dimension while it can expand in the tapered plane. Therefore, the shape of the beam that leaves the TA differs from a ideal Gaussian beam. Reshaping can compensate the ellipticity, however this might still affect the coupling of the light into a single-mode fiber. [30, 7, 31, 18]

The ULE cavity is the basis for a stable and narrow linewidth and is used for the PDH locking. Some characteristics are discussed in the following section 3.2

The idea of the PDH locking and linewidth reduction technique is the conversion of the laser frequency fluctuations into an easy detectable intensity signal that can be used with a PID-controller in a feedback-loop. The transmission signal of the cavity will reach a maximum and the reflectivity goes to its minimum if the laser is on resonance. Every deviation from the resonance frequency causes a change of these signals that can be converted to an error signal by doing side-band modulation of the phase of the laser frequency. [4, 9, 21]

3.2 Ultra Low Expansion Cavity

While an ideal laser is a monochromatic light source, a real laser system suffers frequency fluctuation on different timescales even under laboratory conditions, leading to an unavoidable broadening of the linewidth. Thus, it is crucial to understand the source and effect of the noise in order to be able to address very narrow atomic transitions as we plan it with Dysprosium. The occurring fluctuations are the consequence of different kinds of noise like the change of environmental parameters, vibrations, current instability or unavoidable quantum effects. As it will be discussed later in subsection 4.3.1 it is nearly impossible to prevent the laser from drifting over a range of hours and days. A common way to minimize at least the fluctuations on the short timescale up to milliseconds is to lock the laser to a very stable cavity. Ultra-low expansion cavities (ULE) are normally operated under a stabilized vacuum and are built of a material, usually glass, that is only minimal subjected to temperature induced length fluctuations, so the Finesse can be kept very stable. [6]

3.2.1 Finesse

The finesse of a cavity is the crucial parameter for its quality. This value determines the resulting linewidth of a laser. To outline the relation between the properties of a cavity and its finesse, this subsection gives a very quick reminder of resonator theory. Light at the wavelength λ that enters a cavity of length L will be in resonance if the condition $m \cdot \frac{\lambda}{2} = L$ is fulfilled, where m is an integer. Since there is a usually large but finite number of possible resonant modes, the frequency spacing between two of them is given by the free spectral range (FSR)

$$\nu_{\mathrm{FSR}} = \frac{c}{2\,L\,n} \tag{3.1}$$

that only depends on the length of the cavity L, the speed of light c and the refractive index n inside the cavity. By keeping those parameters as constant as possible, the cavity and thus the laser become very stable. With the spectral width $\Delta\nu$ of one resonant mode, one can calculate the finesse

$$\mathcal{F} = \frac{\nu_{\mathrm{FSR}}}{\Delta\nu} = \frac{\pi\sqrt{R}}{1-R} \tag{3.2}$$

that can also be expressed by the product of the reflectivities R of the cavity mirrors. [6, 10]

3.2.2 TEM Modes

So far, calculating the finesse in subsection 3.2.1 we have only discussed the longitudinal modes in a cavity. However, it is also possible that a small miss-alignment leads to an excitation of higher-order transverse modes, called TEM_{xy} (abbreviation of Transverse Electromagnetic Modes) that can appear within the free spectral range. The subscript denotes the number of nodes in each direction of the two-dimensional plane. The ground mode defined as TEM_{00} is also known as fundamental Gaussian mode, because the two-dimensional transverse profile of electric field and intensity is described a Gaussian. During the characterization of our laser system, several of those transverse modes have been observed and used for locking the laser. The images of these modes shown in Figure 3.1 were taken with a CCD camera that is part of the cavity setup. One can also calculate the shape of these mode, mathematically they are described by Gauss-Hermite modes that are the solutions of the paraxial Helmholtz equation. [6]

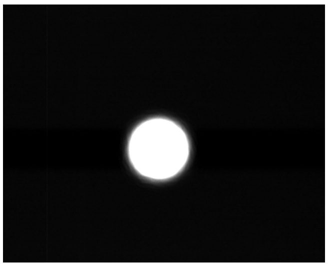

(A) TEM_{00}

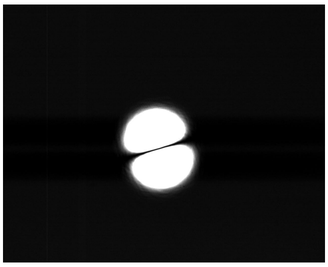

(B) TEM_{01}

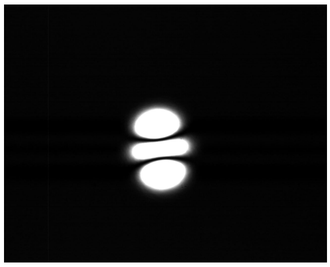

(C) TEM_{02}

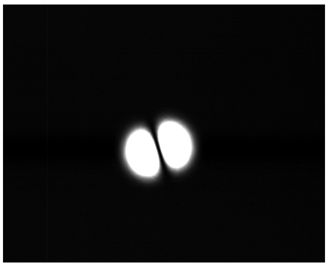

(D) TEM_{10}

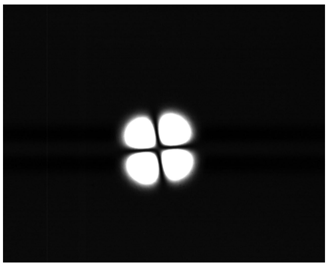

(E) TEM_{11}

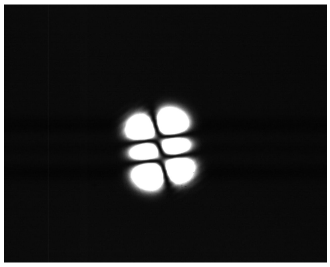

(F) TEM_{12}

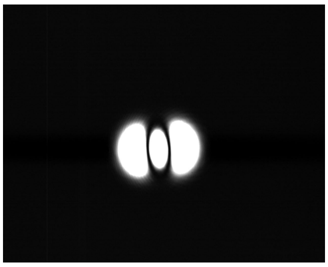

(G) TEM_{20}

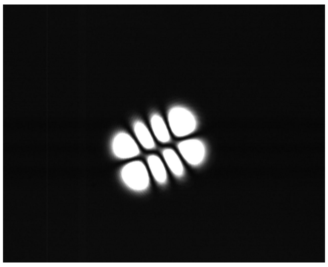

(H) TEM_{31}

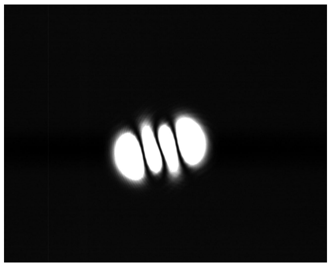

(I) TEM_{30}

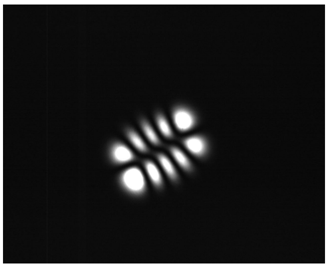

(J) TEM_{41}

FIGURE 3.1: TEM cavity modes that could have been observed and used for laser locking by tuning the piezo voltage within the free spectral range. The fact that 10 different modes appeared implies that the incident beam was not perfectly aligned to the cavity at the moment of capturing the images. The TEM_{00} mode has a Gaussian intensity profile and is the preferred mode for locking. If the light is perfectly aligned to the cavity, it is also the strongest mode.

3.3 Self-heterodyne Linewidth Measurement

The self-heterodyne linewidth measurement is a common method to determine the linewidth of a laser. It uses a kind of Mach–Zehnder interferometer that enables detecting frequency and phase fluctuations as the intensity of an electric field signal on a photodiode. A drawing of the concrete setup can be found in Figure 4.12 together with the application of this method to our laser system in section 4.4. An advantage of this technique is that one does not need any extra laser or other calibrated devices as reference. Instead, a long optical path delay is created by splitting up the laser beam and sending one part through a fiber that is usually tens of kilometers long. The idea of the delayed self-heterodyne linewith method is to create a large delay between two beams of the same laser source, because they can be treated as uncorrelated as a second independent laser would be. The time delay that occurs due to passing a fiber with length l and refractive index n is

$$\tau_\mathrm{d} = \frac{l \cdot n}{c} \tag{3.3}$$

and usually has to be longer than the coherence time $\tau_\mathrm{c} = \frac{1}{\Delta f}$ of the laser to be able to interpret the delayed beam as totally uncorrelated. [14] In this sense, that beam can be treated as a second independent reference laser. The 10.524 km fiber that will be used in this thesis in section 4.4 has a refractive index of $n = 1.467$ [17] resulting in a delay of $\tau_\mathrm{d} = 51.5\,\mu\mathrm{s}$. Especially for narrow linewidth lasers with $\Delta f < 1\,\mathrm{kHz}$ this becomes critical because a much longer fiber would be necessary. For the laser system in this thesis the expected linewidth is below 10 Hz, so theoretically the fiber would have to be at least around 20 400 km long. Nevertheless, it was proven in several papers that even if the beams are not fully uncorrelated, the self-heterodyne method is still a suitable way to estimate the linewith even for ultra-narrow lasers [25, 23, 15, 32]. Note that this method is still an approximation as we neglect $1/f$ noise for instance [22]. The electric field of a laser beam is usually described as the real part of the complex function

$$E(t) = E_0\, e^{i(\omega_\mathrm{L} t + \phi(t))} \tag{3.4}$$

where $\omega_\mathrm{L} = 2\pi f_\mathrm{L}$ denotes the laser frequency and $\phi(t)$ describes phase fluctuations that cause a broadening of the linewidth Δf. Due to the interference of the frequency modulated and the delayed beam, the incident electric field on the photodiode is

$$E_\mathrm{total}(t) = E(t - \tau_\mathrm{d}) + \alpha\, E(t)\, e^{i\omega_0 t}\,. \tag{3.5}$$

The parameter α is a scaling factor that describes the possibly different beam intensities. The additionally $e^{i\omega_0 t}$ term for the beam that has passed the AOM represents the frequency shift by $\omega_0 = 2\pi f_0$. Now we use the Wiener–Khinchin theorem that links the power spectral density of a signal $S(f)$ with its autocorrelation function via the Fourier transformation. Since we also know the proportionality $I \propto |E|^2 = EE^*$ between electric field and intensity, we can calculate the power spectral density on the photodiode

$$S(f) = \mathcal{F}[\langle E_{\text{total}}(t) E^*_{\text{total}}(t) E_{\text{total}}(t+\tau) E^*_{\text{total}}(t+\tau)\rangle](f)\,. \tag{3.6}$$

Under carrying out some more lengthy calculation steps, one finally finds

$$\begin{aligned} S(f) \propto\, & \alpha^2\, e^{-2\pi\Delta f \tau}\, \delta(f - f_0) + \frac{\alpha^2}{\pi} \frac{\Delta f}{(\Delta f)^2 + (f - f_0)^2} \\ & \left[1 - e^{-2\pi\Delta f \tau} \left(\cos\left(2\pi(f - f_0)\tau\right) + \Delta f\, \tau\, \frac{\sin\left(2\pi(f - f_0)\tau\right)}{(f - f_0)\tau}\right)\right] \end{aligned} \tag{3.7}$$

for the expected bet note signal on the photodiode. This relation can be used to estimate the linewidth Δf of the laser. The complete and very detailed derivation can be looked up in reference [2].

4 Characterization of the Laser System

4.1 Optics Setup

The first necessary step to make the laser light usable for a future experimental purpose and the characterization measurements is to set up basic optics. This includes coupling the light into several fibers and planning a permanent setup of optical components to clean and control the polarization and intensity of the laser light, splitting it up into multiple beams and having a possibility to manipulate it. Figure 4.1 depicts a schematic drawing of the installed setup. A single-mode polarization maintaining fiber is connected to the laser's *FiberDock* [28], a special mounting that enables the precise alignment of a lens to couple the light into a fiber. The fiber is lead to a collimator that is placed together with the other optics on a separate breadboard. A half-wave plate in combination with a polarizing beamsplitter is used to adjust the light intensity. Therefore the transmitted p-polarized beam is let through while the reflected s-polarized beam gets blocked. A beamsampler reflects 1 % of the light that gets split up again 50:50 by a beamsplitter providing this small fraction of the light for wavelength and power monitoring. The 99 % of the light remaining is sent through a telescope consisting of two plano-convex lenses possessing a focal length of $f = 150\,\mathrm{mm}$. This is to ensure that the beam diameter[1] is smaller than the active acoustic aperture[2] of the Acousto Optical Modulator (AOM) placed in the telescope's focus. Otherwise the beam could clip and might get deformed. The properties of the used AOM are described in detail in the following subsection 4.1.1. The undiffracted beam gets absorbed in a beam dump, because only the first-order diffracted beam get modulated and shall be further used. Once more, a half-wave plate and a polarizing beamsplitter are used to set the light intensity by polarization adjustment. Lastly, a half-wave plate can be rotated to match the polarization axis of the fiber going to the desired application.

4.1.1 Acousto Optical Modulator

The *Crystal Technology 3110-125* [8] AOM as part of this setup shown in Figure 4.1 enables fast switching and frequency modulation of the laser beam as well as power stabilization or ramping. The AOM consists of a TeO_2 crystal

[1] $w_{\mathrm{calculated}} \approx 220\,\mu\mathrm{m}$
[2] $2.5\,\mathrm{mm} \times 1.25\,\mathrm{mm}$ [8]

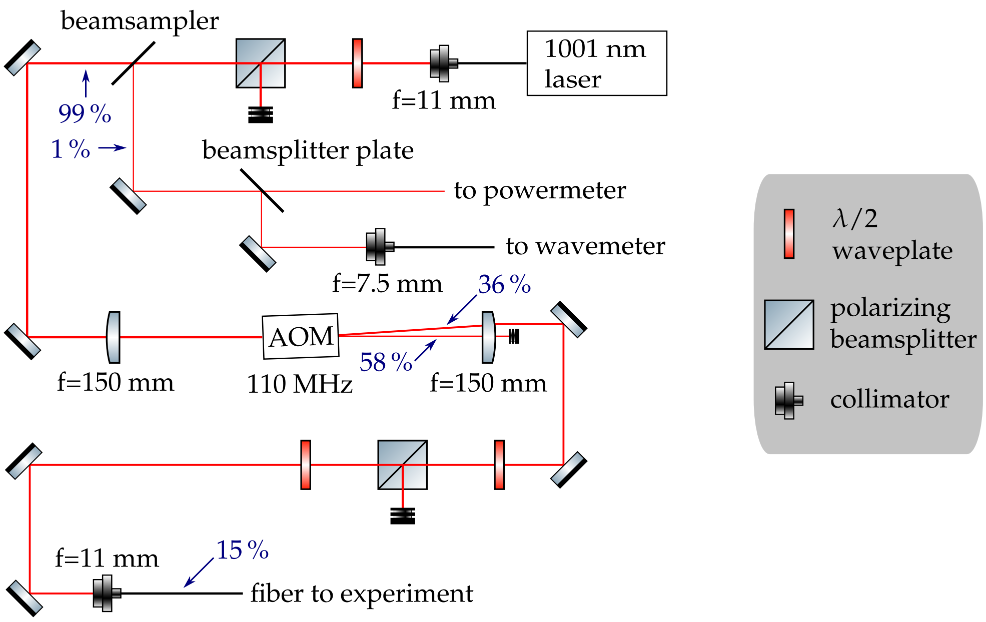

FIGURE 4.1: Schematic drawing of the optics setup for the 1001 nm laser system. A small fraction of the p-polarized light is picked off with a beamsampler and then divided up again to be directed to a photodiode for power-monitoring and to a wavemeter. Before getting to the fiber leading to the experiment, the light passes an AOM that allows for fast switching and fine-tuning of the wavelength. Moreover, it is possible to stabilize and ramp the power going into the experiment. The given percentages refer to the remaining intensity after the corresponding optics component.

that is forced to oscillate with an applied radio frequency f. The structure-borne sound with speed v leads to a local change in density what implies a periodical change of the refractive index n. If the incident light at wavelength λ hits the crystal under the Bragg angle [16]

$$\theta_{\mathrm{B}} = \arcsin\left(\frac{\lambda f}{2nv}\right), \tag{4.1}$$

the light gets partially diffracted and undergoes a frequency shift in first diffraction order of $\pm f$ due to energy and momentum conservation. Higher diffraction orders shifted by $m \cdot f$ $(m \in \mathbb{Z})$ under an angle of $2m \cdot \theta_{\mathrm{B}}$ can also appear, but in general their intensity is weak compared to the zeroth and first order. According to its data sheet, the AOM should be operated with an RF frequency of 110 MHz at around 2 W power. This is realized with a frequency generator[3] set to the desired frequency. Since the signal voltage is limited, its output signal gets amplified by an external RF amplifier[4] to deliver the 2 W power to the AOM. The AOM is designed for wavelengths in a range from 1047 nm to 1060 nm in the near-infrared, so it is not optimal

[3] *RIGOL DG4162*
[4] *Mini Circuits ZHL-1-2W*

coordinated with this laser but is still expected to work with the 1001 nm laser light. Since only the first-order diffracted beam is used, its intensity should be maximized to avoid large power losses. Therefore a comparison of the intensities of zeroth and first-order diffracted beams in relation to the RF power applied to the AOM yields information about the optimal working parameters. Figure 4.2 illustrates the measurement results that characterize the AOM diffraction. These are obtained by adjusting the output voltage of the frequency generator and measuring the diffracted and undiffracted laser beam intensity with a photodiode connected to a powermeter. The first observed tendency was that the first-order diffracted beam gets stronger with increasing power, however it saturates soon and is still less intense than the undiffracted beam even for higher voltages. The zero-order diffracted beam should lose power with nearly the same amplitude as the diffracted one gains it. This is cross-checked by calculating the sum of both intensities that does not change significantly. As an intermediate step the amplifier gain is measured to verify a constant amplification relation between frequency generator signal and amplifier output power that supplies the AOM. It was possible to evaluate a nearly constant amplifier gain of 32.2 dB. Since the frequency generator signal first gets amplified before being sent to the AOM, the actually applied power has to be considered for the efficiency calculations. To do so, the gathered data are processed resulting in Figure 4.2. The plot illustrates the diffraction efficiencies, i.e. the zeroth and first-order diffraction intensity compared to the incident light intensity, relative to the applied RF power which is depicted on the logarithmic dBm scale. As the supplying RF power increases the diffraction efficiency into the first order starts to increase, too. At lower power the change is marginal, but starting at around 20 dBm, a significant improvement in efficiency occurs until the efficiency starts to saturate around 32 dBm. The first-order diffraction efficiency is expected to obey a sine squared function [16]

$$\epsilon = \epsilon_0 \sin^2\left(\frac{\pi}{2}\sqrt{\frac{P_{\text{in}}}{P_{\text{sat}}}}\right), \tag{4.2}$$

depending on the applied power P_{in} and the AOM-specific saturation power parameter P_{sat}. The scaling factor ϵ_0 just determines the maximum reachable efficiency in a real AOM setup where $\epsilon < 100\,\%$. This relation is proven by fitting the function (4.2) to the experimental data represented by the solid line in the graph. The fit parameter modeling the saturation power yields $P_{\text{sat}} = 2.4(1)\,\text{W} = 33.6(4)\,\text{dBm}$. The extrapolation of the fit function emphasizes the observed efficiency saturation and predicts a rapid drop when exceeding the saturation power. The efficiency relation function (4.2) also fits to the diffraction efficiency of the zeroth-order beam when interpreting it as the total intensity minus the first-order diffracted beam and a loss term. Note that the sum of both undiffracted and first-order diffracted beam efficiencies is not equal to 100 % as a small part of the light is diffracted into higher orders and some insertion losses occur as well.

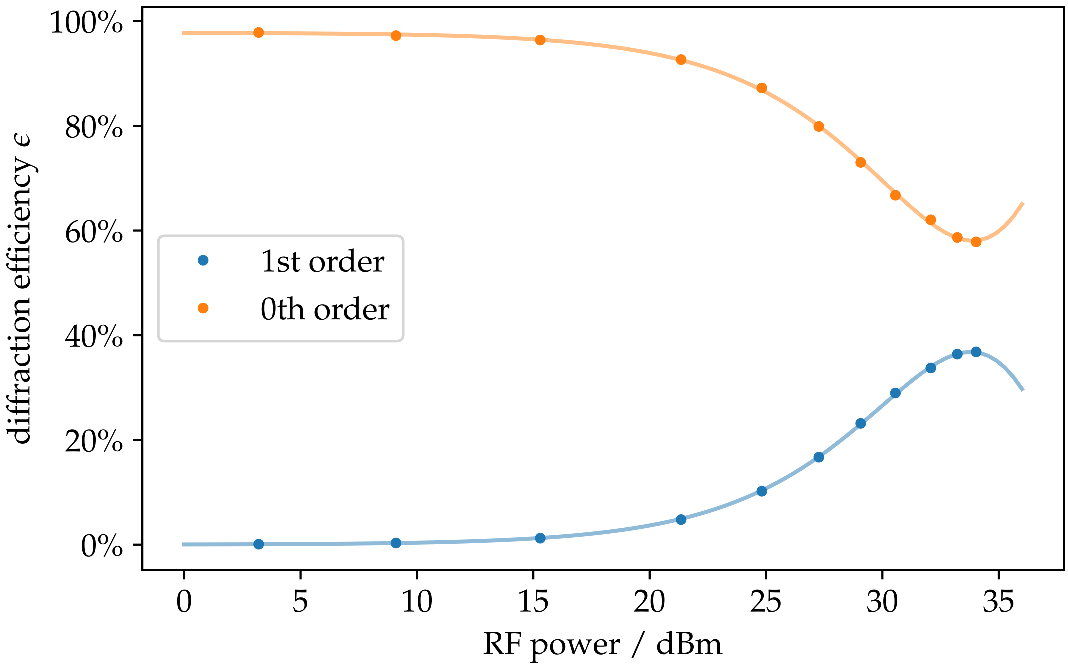

FIGURE 4.2: Illustration of the AOM diffraction characteristics. The diffraction efficiency into the first order increases with the increasing RF power as the depicted sine squared function (4.2) and reaches a maximum of 36 % when saturating at the power $P_{\text{sat}} = 33.6(4)$ dBm according to the fit function parameter. These observations apply analogously to the undiffracted beam efficiency that decreases in the opposite way instead. Due to higher-order diffraction and insertion losses the sum of both graphs is not equal to 100 %.

It has to be concluded that the diffraction efficiency of the first-order diffracted beam is limited to $\sim 36\,\%$ by the current setup and the used AOM. The beam that passes the AOM has already been aligned to optimize the diffraction and its polarization was checked to rule out possible unwanted influences that could reduce the efficiency. The RF power cannot be further increased to improve the efficiency because the applied power should not exceed the determined saturation threshold P_{sat} as a permanent operation of the AOM above this limit will likely lead to damages. Another issue that may contribute to the low efficiency is the shape of the beam leaving the AOM. As the incident beam gets focused down to match the beam size with the active acoustic aperture, the beam is not fully collimated anymore, thus the edges of the beam partially hit the AOM crystal under an angle deviating from the Bragg angle (4.1) [16]. That is why the light does not get fully diffracted and shows an elliptic shape illustrated in Figure A.2g. It has to be made a trade-off between beam shape and size because increasing the beam diameter would cause disadvantages like a longer switching time that goes linear with the beam diameter and the need for more space to set up a telescope with a larger focal length. Consequently, the current AOM should be exchanged by an AOM that is optimized for the light at 1001 nm to reach higher efficiency.

4.1.2 Beam Profile

In general, an ideal laser beam can be described by a Gaussian beam, meaning among other things that its transverse intensity profile

$$I(r,z) \propto \exp\left(-\frac{2r^2}{w^2(z)}\right) \tag{4.3}$$

along the axis of propagation fits a Gaussian function, where $w(z)$ denotes the beam diameter at the position z along the propagation direction and r is the radial distance from the beam center. To have a beam that is in fundamental Gaussian mode, which is equivalent to the TEM_{00} mode already described in subsection 3.2.2, is especially important when using single-mode fibers. Any other intensity distribution profile than the eigenmodes of the Helmholtz wave equation will not be guided properly through this kind of fiber. Note that because of its construction, a Tapered Amplifier does not provide a Gaussian beam, however this is usually compensated before coupling the light into a single-mode fiber [30]. With a *DataRay WinCamD* beam profiler camera [11] it is possible to analyze the laser beam profile at any desired position in the optic path. Using the beam profiler camera is also useful to check the beam diameter when collimating the beam. Therefore, several images of the beam shape were taken that can be found in Appendix A. It could be confirmed that the laser's beam profile is initially in good accordance with the expected Gaussian intensity distribution (4.3). Due to the diffraction at the AOM crystal mentioned in subsection 4.1.1, the undiffracted and the first-order diffracted beam shapes differ from the incident beam. The undiffracted beam gets split into two parts while the first-order diffracted beam is elliptically deformed. Besides the deforming due to focusing the beam, an illustrative approach to explain this behavior would be to argue that since the total light intensity cannot change, the intensity of the diffracted beam has to get "cut out" from the center of the undiffracted beam, therefore it nearly remains no intensity there. As a consequence, the first-order diffracted beam becomes elliptic with a eccentricity of ~ 0.90. As mentioned initially, this is not optimal for the overall efficiency since the elliptic beam causes a large intensity loss when using a single-mode fiber. This reflects the low fiber coupling efficiency of only 15 % noted in Figure 4.1.

4.2 Amplifier Output Power

The Tapered Amplifier (TA) is an important component of the 1001 nm laser system that intensifies the diode seed laser to provide the nominal maximum output power of 2.57 W [29]. The TA itself can be mainly adjusted to set the final laser power by the parameters TA current and TA temperature. Beyond that the seed power as the input parameter determines the resulting power. Therefore, analyzing the relation between current and power respectively temperature and power is part of the laser characterization. The TA current is tuneable in a range from 3.3 A to 6.2 A. For lower currents the laser controller automatically shuts off the emission. This is an internal safety measure, because a TA is a specially shaped semiconductor optical amplifier that has a working threshold similar to a classical diode [30]. When starting the measurement series, the output power was measured at a temperature of $T = 20\,°\mathrm{C}$ with a powermeter placed directly in front of the laser's FiberDock. Figure 4.3 shows the results of the current dependent measurement. When taking a look on this data, one can recognize that starting at approximately $I = 3.7\,\mathrm{A}$ the laser power does not increase strictly anymore but jumps periodically. At some point the power suddenly drops before it stars to increase again. This repeats happening regularly. The data points are connected by a line as a guide to the eye to clearly point out this unexpected non-linear behavior. After the recognition of this unusual performance the measurement was repeated leaving particularly enough time for the parameters to settle before taking the data, but it yielded the same results. At $I = 6\,\mathrm{A}$ the power has only reached 1.2 W, not even half the nominal power. Since the *Toptica DLC pro* laser controller provides an interface to read the laser power detected on an internal photodiode and these values are in line with those from the powermeter, this source is used for the further data acquisition. Decreasing the temperature lead to similar power-current curves. When decreasing the temperature from $T = 20.0\,°\mathrm{C}$ to $19.1\,°\mathrm{C}$, the plot shows a general increase in power. A further reduction of temperature to $18.1\,°\mathrm{C}$ causes a more complex change. Locally, the TA power is now lower than at $19.1\,°\mathrm{C}$ because the two curves are crossing each other at several points where one is falling at this point while the other one reaches a local maximum. However, considering the curve in its entirety the TA output power increases with lower temperature.

Not only a change in current causes these jumps, but also a change in temperature while keeping the current constant affects the power in the same way as Figure 4.4 illustrates. This implies that a change in temperature does not only shift the power by a constant factor as one might have expected regarding the current dependent data in Figure 4.3. Nevertheless, the tendency that the TA power increases when reducing the temperature can be verified. Note that the plot has a broken and differently scaled y-axis to properly depict the widely spread power-temperature curves. It becomes visible that the temperature has less impact on the TA power than the current. Besides, the higher the TA current the larger is the change in power when tuning the temperature. This means that the power drop must be in a way proportional to the current. Neither for the current nor the temperature it becomes evident that there is one single optimal value for which the TA power is maximized independent of the other quantity. Thus, current and temperature always have to be set in adaptation to each other.

As mentioned initially, the TA output power naturally depends on the diode laser seeding power that is adjusted via the diode current. All measurements on current and temperature dependency of the TA power have been taken at a fixed diode current of $I_{\mathrm{diode}} = 156.3\,\mathrm{mA}$ what corresponds to a seed power

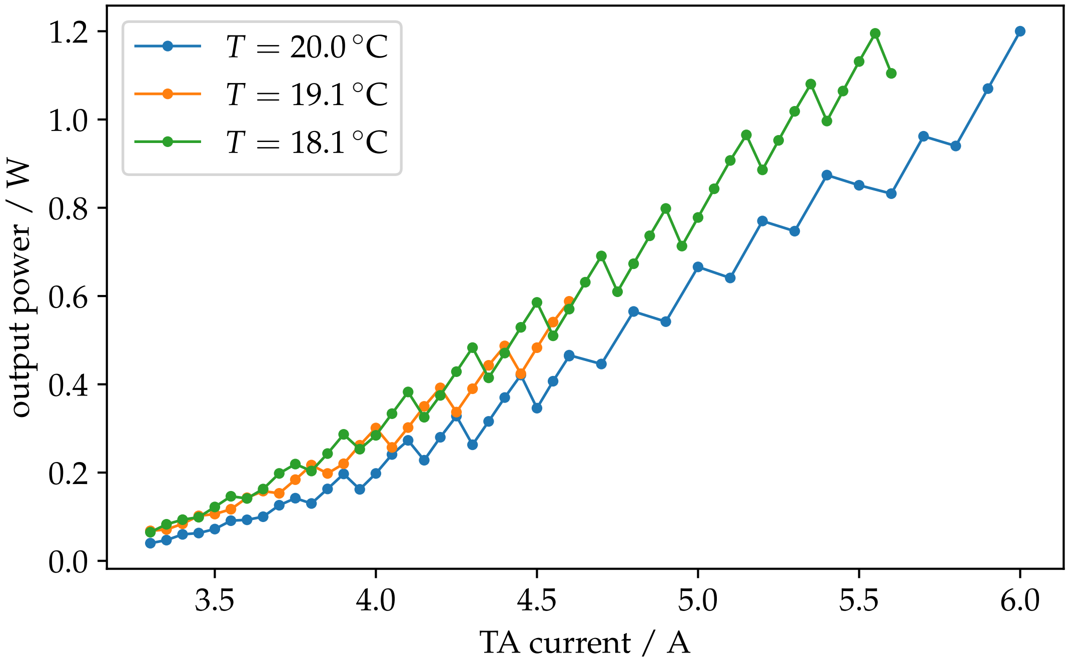

FIGURE 4.3: TA output power relative to the TA current for different TA temperatures but at constant seed power around 50 mW. The output power does not strictly increase all the time with the current but drops regularly what produces a zig-zag pattern. For $T = 20\,°C$ at $I = 6\,A$ the power does not even reach half of the expected value. Decreasing the temperature improves the power in total but still produces a non-linear power-current relation, so for some currents decreasing the temperature can even reduce power.

of approximately 50 mW. Nevertheless, the impact of the diode current respectively the seed power on the TA power should be determined to fully investigate the TAs properties. Figure 4.5 compares the seed power with the TA power relative to the applied diode current. The figure presents a linear relation between diode current and seed. As laser diodes are usually limited in power, this is where a TA finds application. That is reflected by the order of magnitude of seed and TA power. The TA provides around seven times the power that is injected by the diode laser. The diode current can be adjusted in a range from 110 mA to 160 mA. The resulting seed should not exceed 60 mW. These limits arise from the inherent properties of diodes, given by the characteristic curve. Below this value the laser systems shuts off the emission because of a poor injection power. And again, the upper limit is a safety measure to prevent damages. The TA output power starts to increase slower than the seed, but when the diode current goes beyond the threshold at approximately 132 mA, the TA power instantaneously rises and starts to saturate then. It reaches a upper limit that is given by the adjusted TA current and temperature. To ensure a sufficiently injected TA, the laser diode should always be operated with a current $> 140\,mA$, meaning a seed power of approximately 50 mW. Note that there were made some observations that also other parameters than the diode current influence the seed power. By

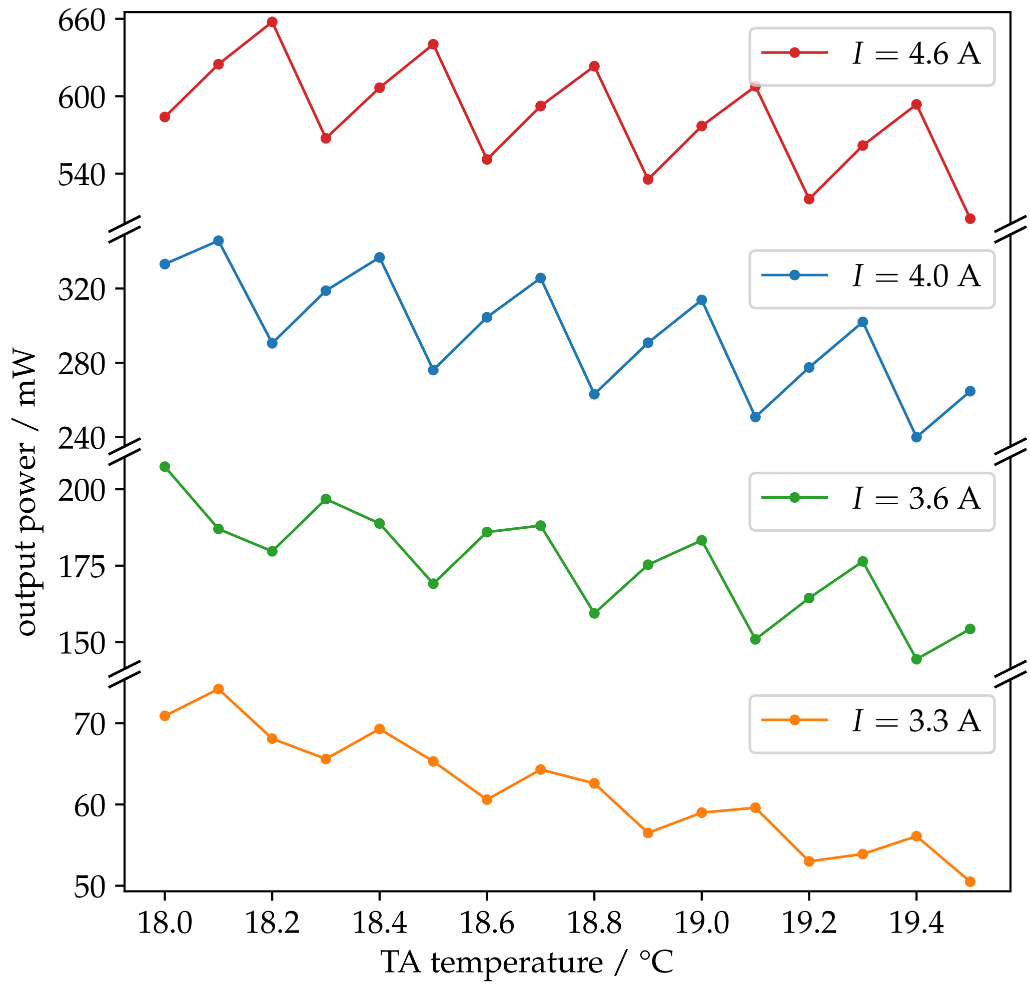

FIGURE 4.4: TA output power against TA temperature for different TA currents but at constant seed power around 50 mW. A change in temperature leads again to a regularly jumping power as observed when tuning the current. The overall tendency is that TA power increases when reducing temperature. The temperature does not enable controlling power as much as the current does. The power fluctuations increase together with the absolute power for higher currents. The positions where the power drops for each current do not correspond to the same temperatures.

increasing the TA current in the usual range from 3.3 A to 6.0 A the seed undergoes a change on the scale of a few mW. A change of the piezo voltage by 10 V caused an increase of 0.2 mW and rising the diode temperature by 0.5 K lead to a change of 0.7 mW. This should not significantly affect the TA power, because the occurred seed fluctuations are in the region where the TA power has already saturated as depicted in Figure 4.5.

Furthermore, a long time monitoring of the amplifier output power at fixed current and temperature revealed that the power also drifts over time, implying that there must be an environmental impact on the TA. Every time the TA power was checked, current and temperature were set to $I = 4.0$ A and $T = 18.1\,°\mathrm{C}$ as well the diode current at 156.3 mA. In average the measured

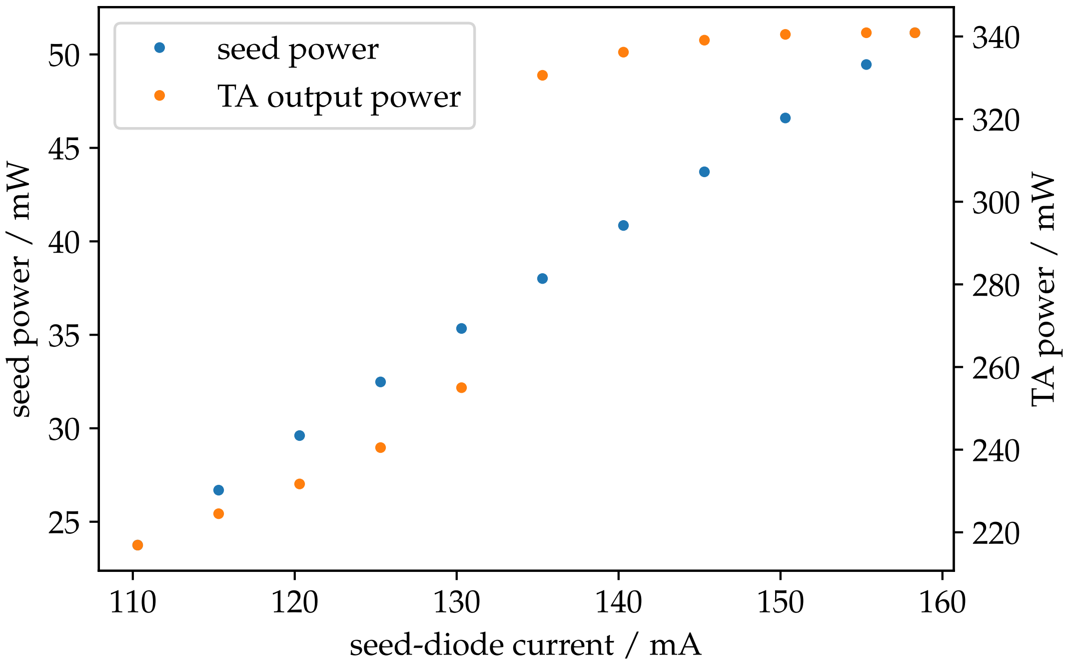

FIGURE 4.5: Comparison of the seed power and the TA output power relative to the diode current for constant TA current $I = 4.0$ A and TA temperature $T = 18.1\,°\mathrm{C}$. The seed power goes linear with the diode current within the working range from 110 mA to 160 mA corresponding to a seed power between 24 mW and 52 mW but never exceed 60 mW. The TA power increases non-linear with the diode current rising instantaneously at a threshold around 132 mA. Above this value the TA power saturates around seven times the seed power, then limited by the TA current and temperature.

power was 352 mW. From this data depicted in Figure 4.6 it can be calculated that over a span of 38 days the power drifted within a range of 102 mW. As a consequence, the data and plots that have been treated in this section so far can only represent a qualitative description of laser system's properties and shall not be understood as absolute values.

Considering these outcomes, the TA performance is not satisfying so far especially because the maximum reachable TA power is far below the expected factory value. The perceived behavior rather indicates that there is an issue with the coupling into the TA-chip. There are methods imaginable to fix this, extending from adjusting some screws up to the necessity to open the laser housing. By precisely optimizing the coupling into the TA's single-mode waveguide region, we expect to be able to achieve a TA power close to the value quoted by the factory. The possibility to improve the output power by adjusting the discussed parameters have been exhausted instead because the currents are set to their upper limits and it is not recommended to set the temperature below 18 °C. Otherwise the temperature might fall below the dew point in case of a high humidity, so the amplifier could get damaged by

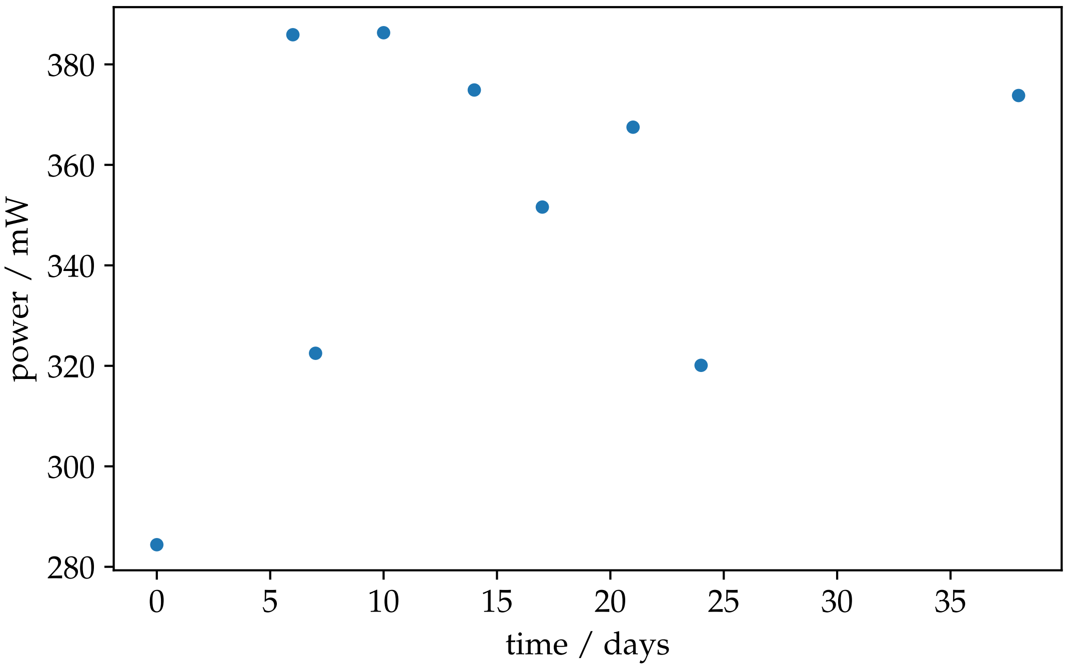

FIGURE 4.6: The laser output power drift was recorded over a range of 38 days, monitoring the current output power in average every 5 days. The laser system's parameters were always set to the same fixed values as well for the TA current $I = 4.0\,\mathrm{A}$ and temperature $T = 18.1\,°\mathrm{C}$ as for the diode current $I_{\mathrm{diode}} = 156.3\,\mathrm{mA}$ ($\sim 50\,\mathrm{mW}$ seed). The randomly appearing drift over a range of 102 mW indicates that the laser power correlates with some external influences, likely a environmental factor that impacts the coupling efficiency of the seed light into the TA.

moisture[5]. Meanwhile, the non-linear increasing TA power is less problematic since there are other options to control and stabilize the laser power in the optic setup as the installed AOM or the half-wave plates and beamsplitters.

4.3 Wavelength

The wavelength of the free running laser can be set via the three independent parameters piezo voltage, diode temperature and diode current. The absolute values that will be presented in the figures in this section are not reproducible since the wavelength is sensitive to environmental changes and therefore drifts over time if the laser is not locked. For further details refer to subsection 4.3.1. The wavelength monitoring is realized with the installed optics setup Figure 4.1 and a *HighFinesse WS6-600* wavemeter [13]. As this laser system shall be used for high-precision spectroscopy of ultra-cold dysprosium, the aim is to set the wavelength of the laser to the desired transition wavelength nearby 1001 nm. For the ^{162}Dy isotope the exact transition wavelength is 1000.9034 nm according to the NIST database [19]. The most practicable and therefore frequently used way to adjust the wavelength is to

[5] Note that some parts of the TA, i.e a Peltier element, might be colder than 18 °C.

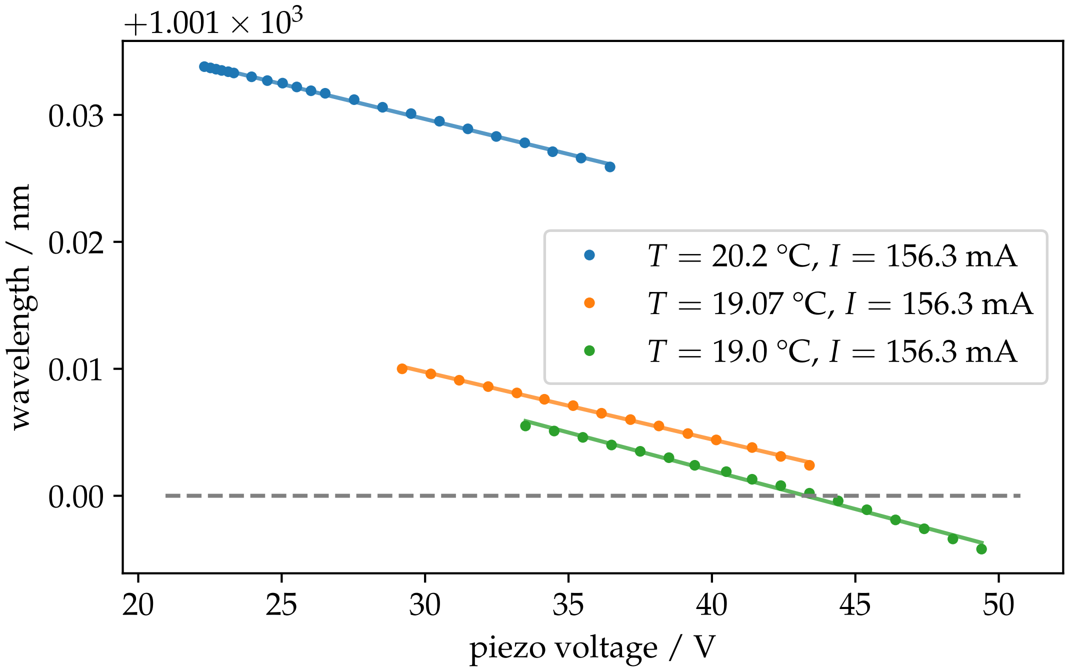

FIGURE 4.7: Wavelength as a function of the piezo voltage at different diode temperatures but constant diode current. The solid lines represent linear fit functions to determine the proportionality constant $-5.5(3) \times 10^{-4}$ nm/V and the dashed line marks the target wavelength of 1001 nm. For a diode temperature of 20.2 °C within the studied piezo voltage range the wavelength is close but still 3×10^{-2} nm away, so a piezo voltage even higher than 50 V would be necessary to get to the desired value. Reducing the temperature to a value around 19 °C enables getting to 1001.000(2) nm with respect to the accuracy of the wavemeter.

tune the piezo voltage. Figure 4.7 contains the wavelength change resulting from a variation of the piezo voltage under different settings of the remaining relevant parameters. Note that the diode current was kept constant at 156.3 mW except for the separate study of this parameter later on. In general, the first finding is that the wavelength can be reduced by increasing the piezo voltage and vice versa. Initially, while the diode was set to a temperature of 20.2 °C and the piezo voltage running in a range from 22 V to 36 V, the required wavelength of 1001 nm was not reached, still deviating by ~ 0.03 nm from the dashed reference line. It might be possible to get to the desired value but this would require an immense increase of the piezo voltage. Reducing the temperature to 19.07 °C helped to reduce the remaining difference of the current wavelength to the reference value to the order of 10^{-3}, however at $U = 44$ V the wavelength did still not match 1001 nm. A slight reduction of the temperature to 19 °C enabled reaching the 1001 nm at a piezo voltage of 43.5 V. This proves that it is possible to set the wavelength to 1001.000(2) nm or another close value with regard to the given accuracy of the wavemeter of 500 MHz. A linear fit to the data, that is represented in the plot by the solid lines, enables to determine the proportionality factor of $-5.5(3) \times 10^{-4}$ nm/V between wavelength and piezo voltage. Note that this

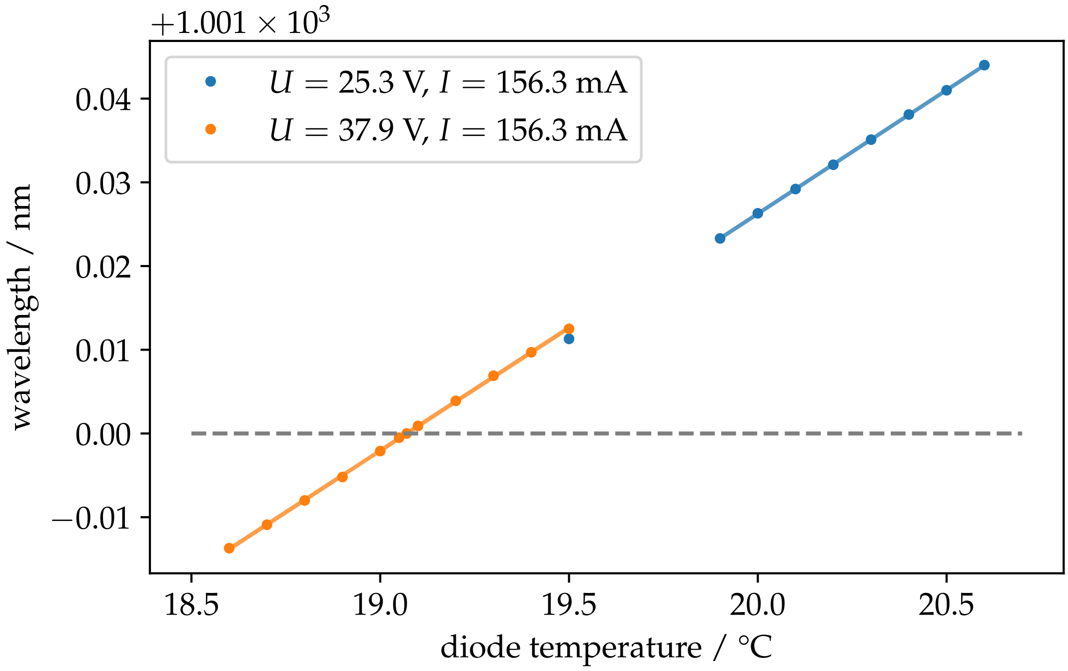

FIGURE 4.8: Wavelength in relation to the diode temperature at different piezo voltages. The wavelength increases with increasing temperature by $2.9(1) \times 10^{-2}$ nm/°C. This value was determined by a linear fit function depicted by the solid lines. The impact of the piezo voltage compared to the temperature is small. A 12.6 V change in the piezo voltage did not lead to a visible displacement between the accompanying curves. Around 19 °C the wavelength crosses the dashed line marking the reference value 1001 nm .

is an average value of all measurements where the slopes were reasonably constant.

As it was already deduced that a reduction of the diode temperature also reduces the wavelength, it remains investigating the quantitative relation. From Figure 4.8 it becomes obvious that a change in temperature leads to a larger wavelength change than it has been observed with the piezo voltage. Comparing the data at $U = 25.3$ V and 37.9 V, it seems that both lines merge into each other. This is verified by the proportionality factor $2.9(1) \times 10^{-2}$ nm/°C that is two orders of magnitude larger than the one for the piezo voltage. The data also reveal that the diode temperature should be set to approximately 19.0 °C to reach the desired wavelength withing a piezo voltage range between 30 V and 50 V. The confrontation of piezo voltage and diode temperature emphasizes their fields of usage. The diode temperature enables coarse tuning of the wavelength. Therefore it has not to be changed frequently. This meets with the fact that the diode temperature needs a longer time to settle than the piezo voltage does until providing a stable wavelength. Thus, the piezo voltage is the optimal parameter for fast and frequent fine-tuning of the wavelength. Note that, because of this, when it comes to locking the laser the piezo voltage is going to be used for selecting one of the cavity modes (see subsection 3.2.2), so it comes to a restriction of this value.

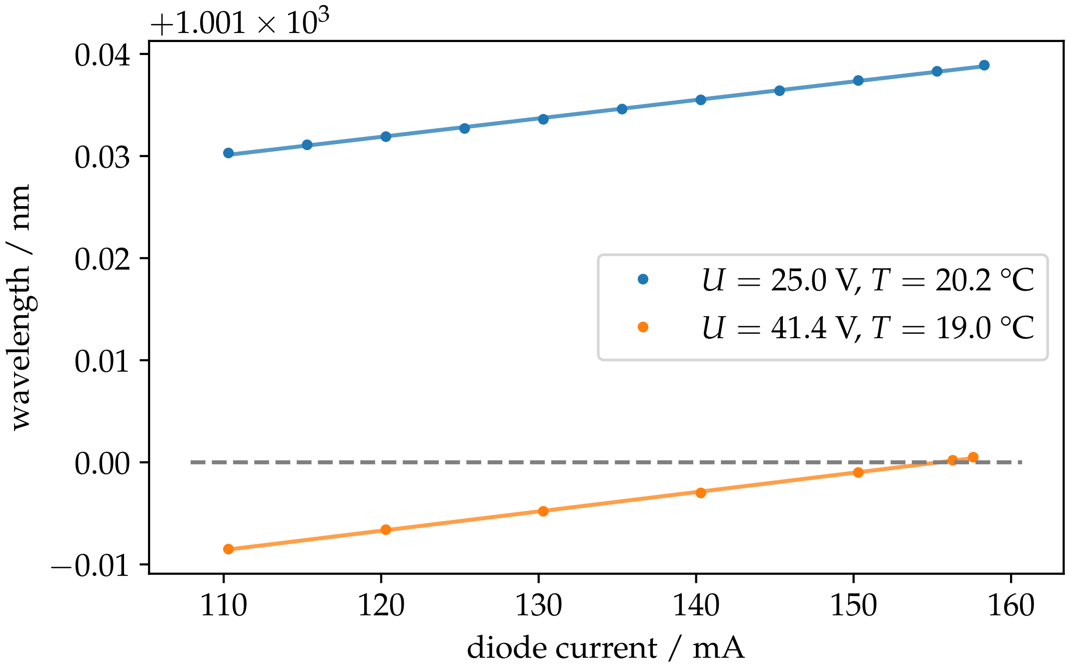

FIGURE 4.9: Wavelength dependency on the diode current at different diode temperatures and piezo voltages. The diode current is limited to the depicted range between 110 mA and 160 mA. For $U = 25.0\,\mathrm{V}$ and $T = 20.2\,°\mathrm{C}$ the wavelength does not match the required value of 1001 nm marked by the dashed line. Optimizing the the piezo voltage and the diode temperature to $U = 41.4\,\mathrm{V}$ and $T = 19.0\,°\mathrm{C}$ enabled reaching the desired wavelength for the required diode current of 156 mA. The solid lines represent a linear fit function that yields a slope of $1.9(1) \times 10^{-4}\,\mathrm{nm/mA}$.

Although the diode current, which was kept constant during the previous measurements, also affects the wavelength, this parameter should not be used with the intention to change the wavelength because the diode current is mainly responsible for the sufficient seeding of the TA as it was explained in section 4.2. Nevertheless, the impact of the diode current on the wavelength was investigated for the sake of completeness resulting in Figure 4.9. As mentioned earlier, the diode current is limited to the range from 110 mA to 160 mA because of the TA seeding. For a diode temperature of 20.2 °C and a piezo voltage of 25.0 V, the target wavelength is out of range by at least $3 \times 10^{-2}\,\mathrm{nm}$. Changing the parameters to $T = 19.0\,°\mathrm{C}$ and $U = 41.4\,\mathrm{V}$ is an optimization to reach the 1001 nm at the usual diode current 156 mA. The linear fit functions yield a proportionality factor of $1.9(1) \times 10^{-4}\,\mathrm{nm/mA}$ which is in the same order as the one for the piezo voltage.

A listing that contains again all the determined proportionality factors which describe the relation of the wavelength to piezo voltage, diode current and temperature can be found in Table 4.1.

Parameter	Proportionality	
Piezo voltage	$-5.5(3) \times 10^{-4}$	nm/V
Diode temperature	$2.9(1) \times 10^{-2}$	nm/°C
Diode current	$1.9(1) \times 10^{-4}$	nm/mA

TABLE 4.1: The wavelength depends linear on the piezo voltage, the diode temperature and the diode current. The diode temperature causes the largest change. The impact of piezo voltage and diode current is two orders of magnitude smaller. Wavelength decreases with increasing piezo voltage but increases with rising diode temperature and current. Piezo voltage is suitable for fine tuning, diode temperature for coarse tuning. Diode current should not be changed due to required constant seed power.

4.3.1 Wavelength Drift

A comparison of the three different plots in section 4.3 reveals that although there are configurations for which the parameters are identical, the wavelength varies. This is the consequence of the normal drift of the wavelength that occurs to the unlocked laser over time due to environmental impacts. To systematically describe this drift, the wavelength was monitored in total over 14 hours. Figure 4.10 compares the recorded wavelength data with the course of air pressure, temperature and humidity during the measurement to identify possible correlations. When starting the recording, piezo voltage and diode temperature were set to $U = 45.4\,\mathrm{V}$ and $T = 19.0\,°\mathrm{C}$ to ensure that the wavemeter displays a wavelength of 1001.0000 nm. The reason for the decreasing wavelength in the very beginning is that the piezo voltage needed around 3 minutes to even out at 46.8 V. After that very short drop, the wavelength continuously increased over time by 5.6×10^{-4} nm in 6.6 hours or 168 MHz expressed as a frequency drift. It is probable that the wavelength correlates with the air pressure because it increased also nearly constant in the same time. Temperature and humidity show a more complicated behavior. For a while they stay nearly constant, but then there are periods when a large increase or decrease occurs. However, there is no significant change of the wavelength's behavior observable at the same time, thus they likely do not influence the wavelength. A possible reason might be that inside a temperature stable wavemeter apparatus only air pressure fluctuations can cause a change of the refractive index of the air. The observed behavior repeats similarly when monitoring the wavelength again 4 days later, then the wavelength drifted by 6.1×10^{-4} nm in 7.3 hours or 183 MHz in units of frequency. This time the wavelength drop at the beginning of the measurement is even larger. This is because the diode temperature was changed to 18.9 °C and the piezo voltage to 43 V initially, because the wavelength has already drifted 1×10^{-3} nm away from 1001 nm under the previous settings. Since the piezo voltage did not stay absolutely constant all the time, a possible contribution of these fluctuation to the wavelength drift cannot be ruled out. A maximum deviation of 0.4 V was recognized, when the piezo voltage increased over time. Taking into account the in section 4.3 determined proportionality of $-5.5(3) \times 10^{-4}$ nm/V, this effect would have forced the wavelength to decrease by 2.2×10^{-4} nm although it increased all the time. Consequently, the observed drift did more likely depend on the air pressure than the piezo voltage. The average wavelength drift of 25 MHz per hour is close to the wavemeter's resolution of 20 MHz but since the drift continuously occurred over 14 hours, it is very likely that the recorded data represent the actual drift.

If the laser is locked, we instead expect the wavelength to do not change significantly over time. To prove this assumption, the wavelength recording was also done when the laser was locked to the TEM_{00} mode for roughly one hour. Due to the locking to this cavity mode, which can be found by tuning the piezo voltage, the wavelength cannot be set independently anymore. That is the reason why the piezo voltage has to be set to 51.08 V at $T = 18.9\,°C$ what leads to a wavelength of 1001.0032 nm as Figure 4.11 presents. The wavemeter has a deviation sensitivity of 20 MHz corresponding at 1001 nm to a resolution of 6.7×10^{-5} nm. Since the detected fluctuations are within 4×10^{-5} nm and therefore smaller than the device resolution, the recorded data do mainly contain digital noise. This means that we cannot determine the wavelength stability of the locked laser more precise than to 6.7×10^{-5} nm. This value is at least an approximation for it. At the factory, the measured cavity drift was 440 mHz/s [27] and it was mentioned that this value should reduce over time. We could not experimentally check this, but when locking the laser to the ULE cavity one can assume that the wavelength drift should be in accordance with this value.

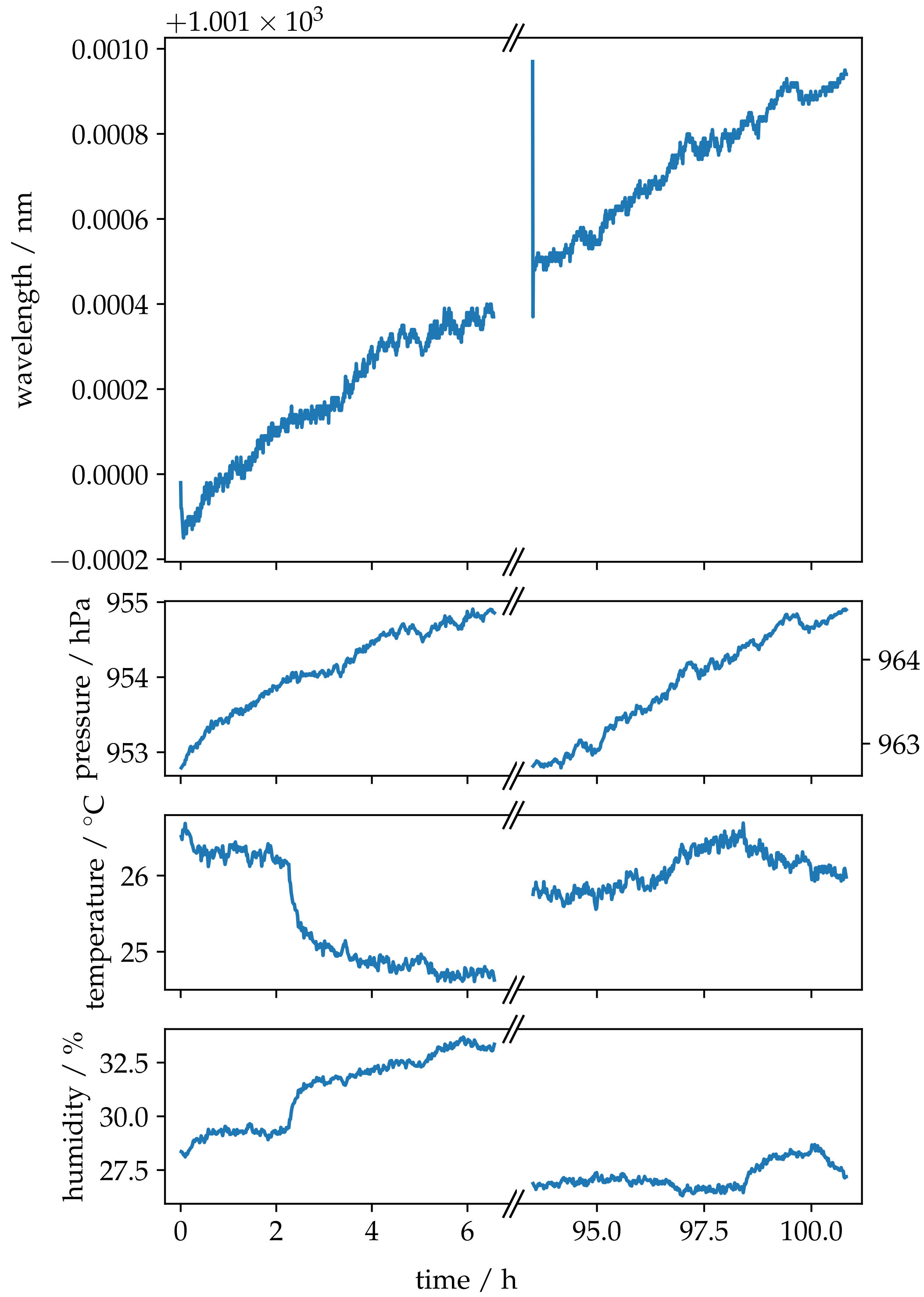

FIGURE 4.10: The wavelength drifts by 8.4×10^{-5} nm or 25 MHz per hour. The data were taken over 13 hours in total within 4 days and are shown in comparison to the environmental conditions. The resolution of the wavemeter is 20 MHz. The immediate dropping wavelength at the beginning of the measurements is caused by the initial change of parameters that start to settle then. At $t = 0$ h the piezo voltage was set to 45.4 V and the diode temperature to 19.0 °C. The parameters were then changed at $t = 93.5$ h to $U = 43.0$ V and 18.9 °C before recording again. As temperature and humidity show complicated courses and only the air pressure behaves similar to the wavelength, this factor seems to correlate with the wavelength drift.

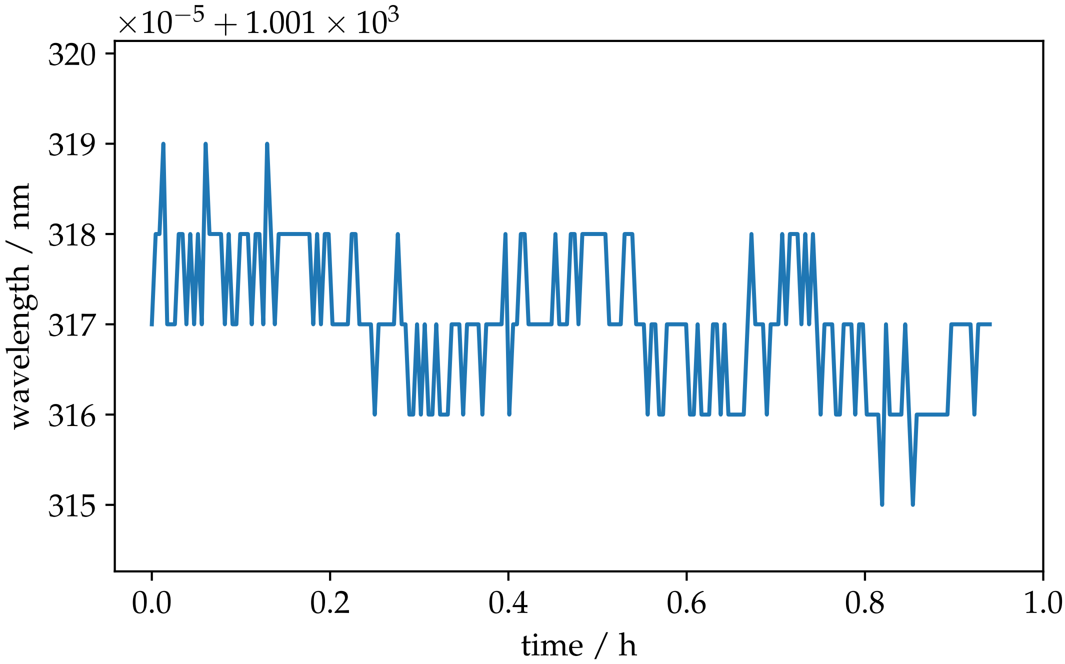

FIGURE 4.11: The wavelength seems not to drift more than 4×10^{-5} nm when the laser is locked. These data are not reliable and contain noise because they predict a drift smaller than the wavemeter's resolution of 20 MHz respectively 6.7×10^{-5} nm at 1001 nm. Nevertheless, the wavelength stability can be approximated to this value.

4.4 Linewidth

The ultra-narrow linewidth is the key feature of this laser system. In this section the laser linewidth is going to be estimated using the delayed self-heterodyne method to verify the expected value quoted by the manufacturer.

4.4.1 Measurement Setup

The in section 3.3 introduced delayed self-heterodyne linewidth measurement method is realized using the setup schematically drawn in Figure 4.12. This was already assembled during an earlier thesis at the PI5 [2], but some critical optics components had to be exchanged to adapt to the specific wavelength of our laser system. The laser light is provided by a fiber coming from the setup shown in Figure 4.1. The intensity division into the two arms of the interferometer can be adjusted with a half-wave plate in front of a polarizing beamsplitter. One part of the light undergoes a frequency modulation of 80 MHz in first diffraction order generated by an AOM[6]. The second beam passes a 10.524 km long single-mode fiber[7] to create a sufficient delay between the two beams with the aim to treat them as mostly uncorrelated. Both beams then are brought to interference by overlapping them. This is done again with a polarizing beamsplitter. Equalizing the intensities can be

[6] *Crystal Technology 3080-120 6300*
[7] *j-fiber IG-09/125/250*

done by adjusting a half-wave plate. The power spectral density of the beat note signal shall be detected with a fast photodiode[8] and analyzed on an oscilloscope, therefore the beam size gets reduces and the contributions of the perpendicular polarization components get equalized.

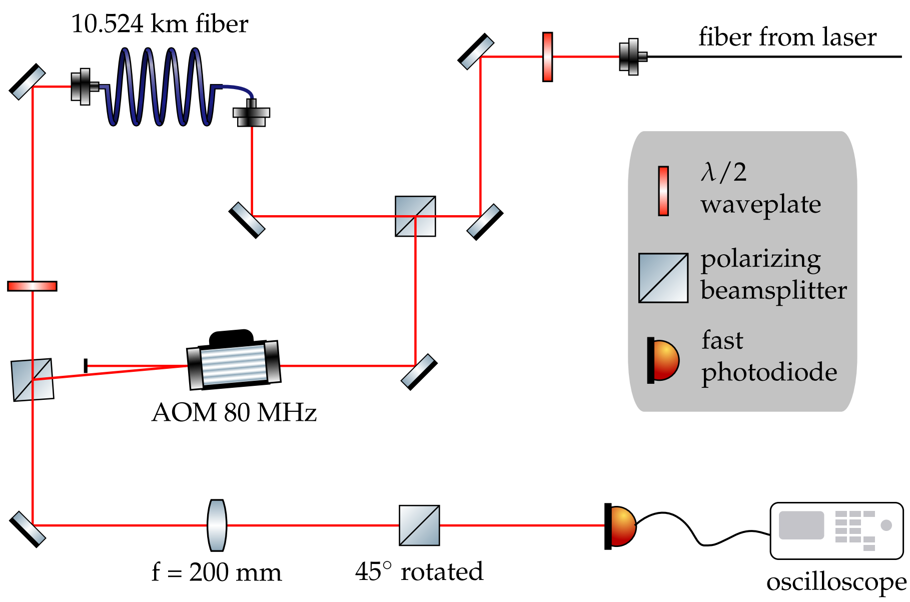

FIGURE 4.12: Scheme of the setup to determine the laser linewidth via the self-heterodyne linewidth measurement. The laser light gets split up into a Mach-Zehnder like interferometer where one beam is frequency shifted by 80 MHz because of passing an AOM and the other arm undergoes a time delay of $\tau = 51.5\,\mu s$ while passing a 10.524 km long fiber. Both beams will then interfere after being superimposed again. The resulting beat note spectrum is detected with a fast photodiode and monitored on an oscilloscope.

4.4.2 Experimental Results

Both interferometer arms have to be precisely aligned to the beamsplitter with the aim to perfectly overlap for a strong beat note signal on the photodiode. Furthermore, the laser has to be locked to see the full interference pattern. A spectrum analyzer[9] was used to recognize and optimize the beat note spectrum during the alignment. The advantage of this device is that the signal is already depicted as the frequency dependent power spectral density on the screen. It was possible to observe the expected frequency spectrum [22] with a larger peak centered at the AOM frequency of 80 MHz and many smaller peaks with decreasing intensity the more they are away from the center. With the recorded data in Figure 4.13, a first estimation of the linewidth was possible fitting the in section 3.3 deduced frequency dependent function (3.7) to the measured signal having the linewidth Δf and the

[8] *Thorlabs PDA015C/M*
[9] *HAMEG HMS3000*, in this case 400 Hz frequency resolution

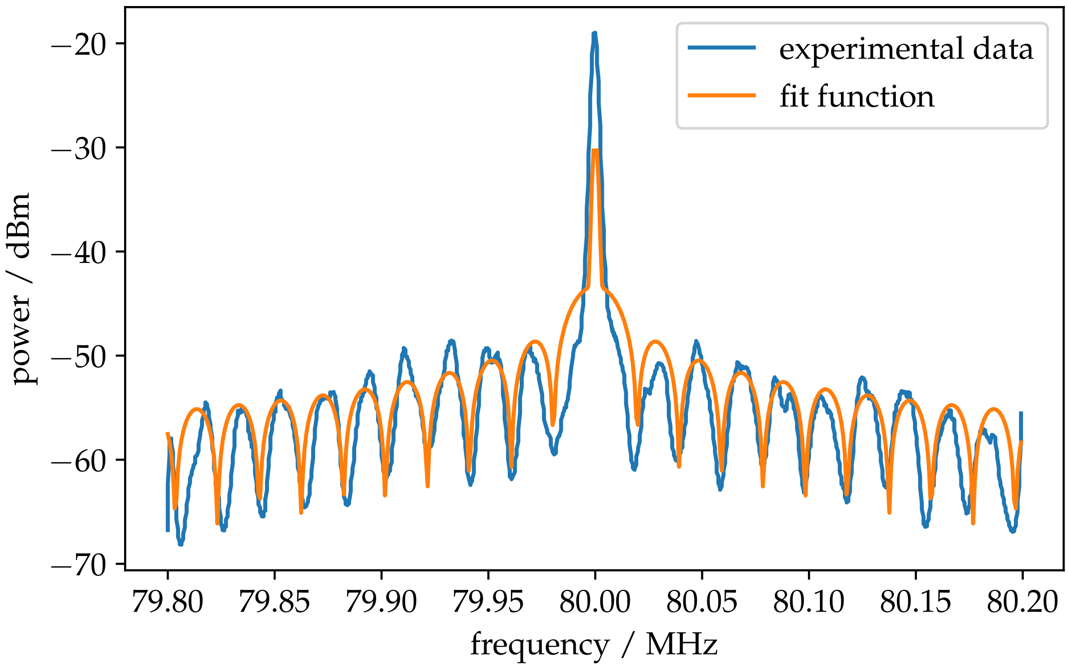

FIGURE 4.13: The power spectral density of the beat note signal obtained from the laser light interference in self-heterodyne linewidth measurement was taken with a spectrum analyzer. For the determination of the linewidth, applying the fit function (3.7) yields $\Delta f = 10\,\mathrm{Hz}$. This is only a first estimation since the spectrum has to be recorded with a higher resolution to reach a more precise value. The experimental data are not perfectly in accordance with the fit but spacing and height of the single peaks matches in average.

delay time τ_d as fit parameters. One can see that the fit function does not perfectly match the observations, but the spacing and the average height of the individual peaks is in good accordance with the original signal. The fit parameters yield $\Delta f = 10\,\mathrm{Hz}$ for the linewidth and $\tau_\mathrm{d} = 52.6\,\mu\mathrm{s}$ for the delay time, being in accordance with the acceptance report that specifies the linewidth to be smaller than 10 Hz and the delay time also fits quite good to the calculated value of 51.5 µs. To go beyond this initial guess, the spectrum analyzer was replaced by a high-resolution oscilloscope[10] to record the intensity variations on the photodiode. For the analyze of the beat note spectrum, the recorded time dependent signal has to be transformed to the frequency dependent Fourier space via the numeric fast Fourier transformation (FFT). With the chosen sampling rate, the spectral frequency resolution was 20 Hz in this case. Again, the recorded signal shows some noise and therefore does not exactly match the fit function (3.7) especially at the centered peak, however the properties of the multiple smaller peaks should be respected quite good. In this case, evaluating the fit parameters gives a linewidth of $\Delta f = 6.7\,\mathrm{Hz}$ that meets the condition of the acceptance report.

The setup for the self-heterodyne linewidth measurement cannot only be used to detect the beat note signal of the very narrow locked laser but also

[10] *LeCroy WaveRunner 64Xi*, sampling rate set to 200 MS/s

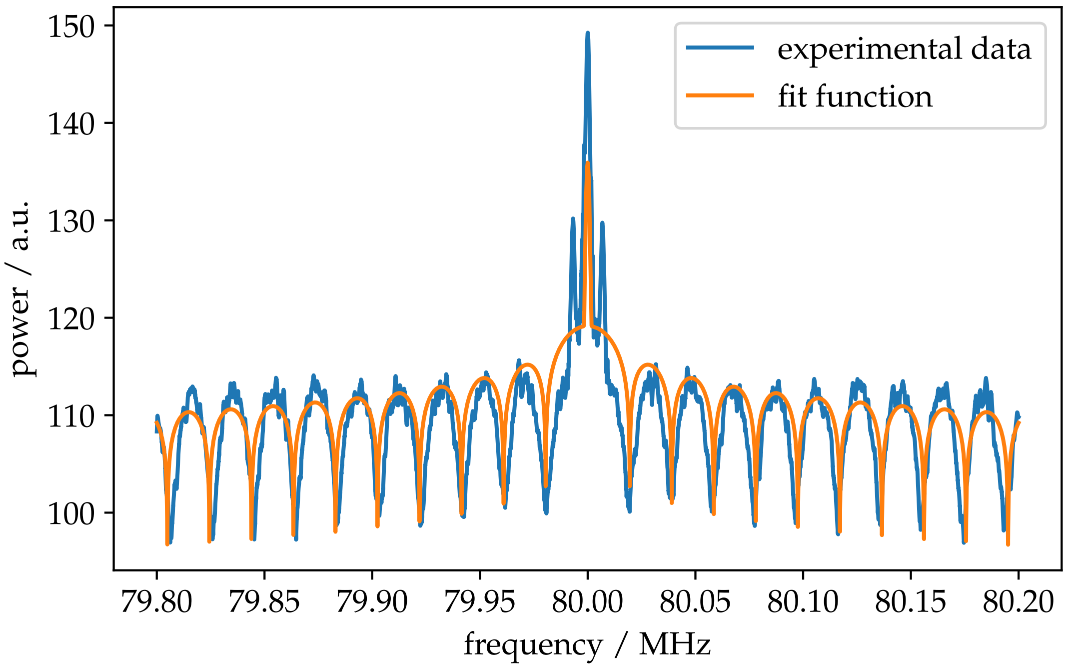

FIGURE 4.14: Power spectral density of the beat note signal taken with an oscilloscope at 20 Hz resolution. The higher resolution causes slightly more noise than occurring with the spectrum analyzer (Figure 4.13). Applying the fit function (3.7) still matches reasonably and yields $\Delta f = 6.7\,\text{Hz}$ for the linewidth.

works for free running laser. However, in this case the power spectral density does not obey the function (3.7), but we expect to observe a Voigt profile that is a convolution of Gaussian and Lorentzian and is a consequence of the interaction of white and $1/f$ noise. A result of the convolution is that the Voigt integral cannot be solved analytically, but one can use a so called pseudo Voigt function that is a sufficient approximation to it. From this fit function illustrated together with the interference signal of the unlocked laser in Figure 4.15, one can estimate the linewidth of the free running laser to be around 50 kHz. Compared to other lasers this result underlines the narrow linewidth of our laser system since other lasers do not reach this value even if they are locked.

Finally, to check the plausibility of the experimentally determined linewidth and to rule out possible disturbing influences, the spectra of the involved RF components were investigated. An unintentional broadening of the laser linewidth due to a too broad AOM supplying signal could distort the whole linewidth measurement or even make it useless. Analogously to the description in subsection 4.1.1, the AOM in this setup is supplied by a combination of frequency generator[11] and external RF amplifier[12]. One occurring effect was that one could always see a background peak of the 80 MHz signal driving the AOM that became especially visible when there was no interference

[11] *RIGOL DG4162*
[12] *Mini Circuits ZHL-3A-S+*

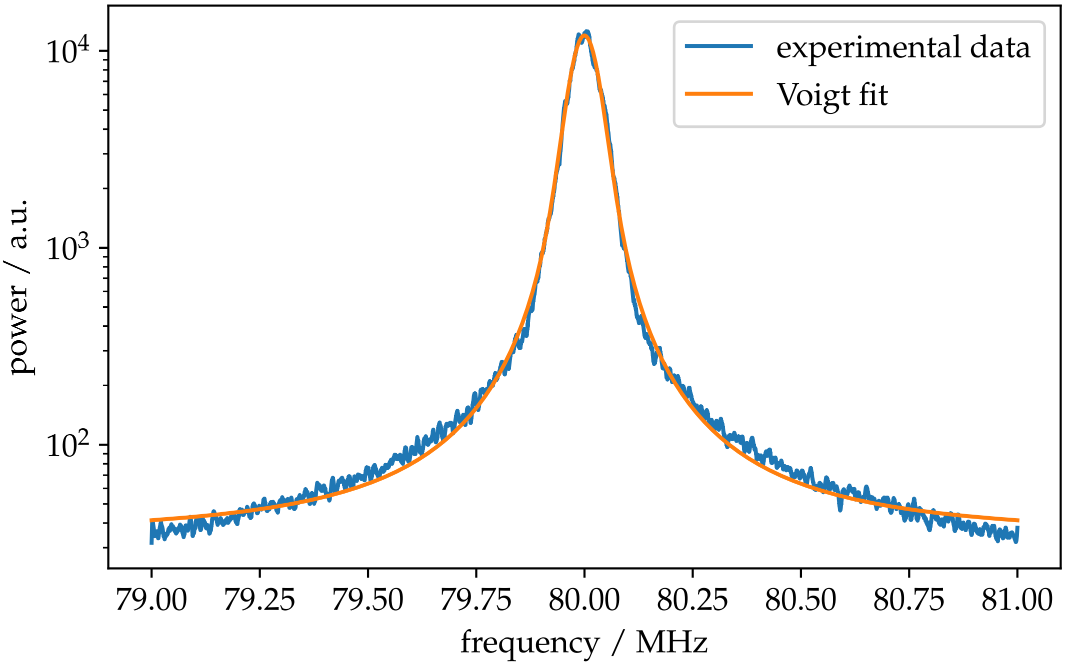

FIGURE 4.15: Beat note spectrum of the free running laser. The power spectral density is much broader compared to the locked laser. The periodic beat note pattern has disappeared, instead the signal looks like a Voigt profile possibly caused by the more dominant $1/f$ noise. A pseudo Voigt profile fit function can be used to estimate the linewidth $\Delta f \approx 55\,\mathrm{kHz}$.

of the both beams at this moment. Placing the RF amplifier farther away from the interferometer setup solved this issue. Nevertheless, the spectra of frequency generator and amplifier were captured with the oscilloscope the compare the width of their output signal as it is shown in Figure 4.16. A obvious difference of the peaks' width cannot be recognized as well as the Gaussian fit functions verify that both peaks have a FWHM of approximately 40 Hz. It can be noticed that the actual signal is not a real Gaussian, however we can use this approximation to estimate the frequency width. The determined bandwidth influences the frequency shift and the linewidth of the beam that passes the AOM and therefore defines the exact center position of the beat note spectrum. The estimated bandwidth and the accordance between frequency generator and amplifier indicate that there should not be a significant influence on the estimated linewidth, however one should keep in mind the the discussed result for the linewidth is subjected to several unavoidable uncertainty factors.

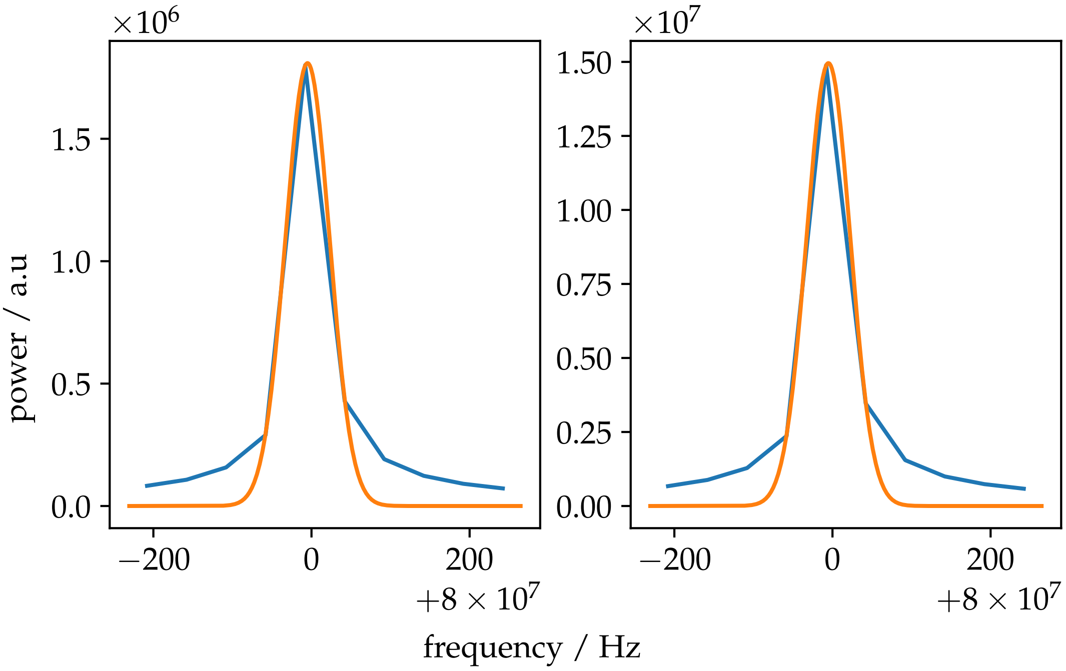

FIGURE 4.16: The signal spectra of the frequency generator (left) and the RF amplifier (right) were captured to determine the bandwidth of the AOM supplying signal by using a Gaussian fit function (orange curves). Their bandwidth is approximately 40 Hz. This helps to analyze possible broadening effects of the laser's linewidth that cannot be ruled out but should not have significantly larce impact. The resolution is limited by the sampling rate.

4.5 Ring-down

The cavity ring-down spectroscopy is a technique to determine the lifetime of the photons and out of that the finesse of a cavity [10, 6]. The basic idea is to interrupt the incident light to the cavity with a fast switch while measuring the transmission signal of the cavity simultaneously. Due the the usually high finesse and therefore reflectivity of the mirrors in a cavity one expects to still have photons in the cavity, but they will decay exponentially after switching off the incident light. From this decay one can determine the lifetime of the photons. In case of this laser system an EOM modulates the light that goes into the cavity. Thus, one can take advantage of the short switching time of an EOM, so we interrupt the supplying RF signal to control the ring-down measurement. A simple TTL logic switch is connected to the logical input of an RF switch[13] that can switch the EOM driver signal. Before carrying out the ring-down, one has to verify that the RF switch is fast enough to switch off the EOM faster than the expected decay which is given in the acceptance report with around 44 µs [29]. Figure 4.17 contains the test measurement results when observing the switching of an 80 MHz RF signal on an oscilloscope and triggering with the TTL signal. At $t = 0$ the TTL control signal exceeds the threshold voltage for the recognition of a logical HIGH

[13] *Mini-Circuits ZSDR-230+*

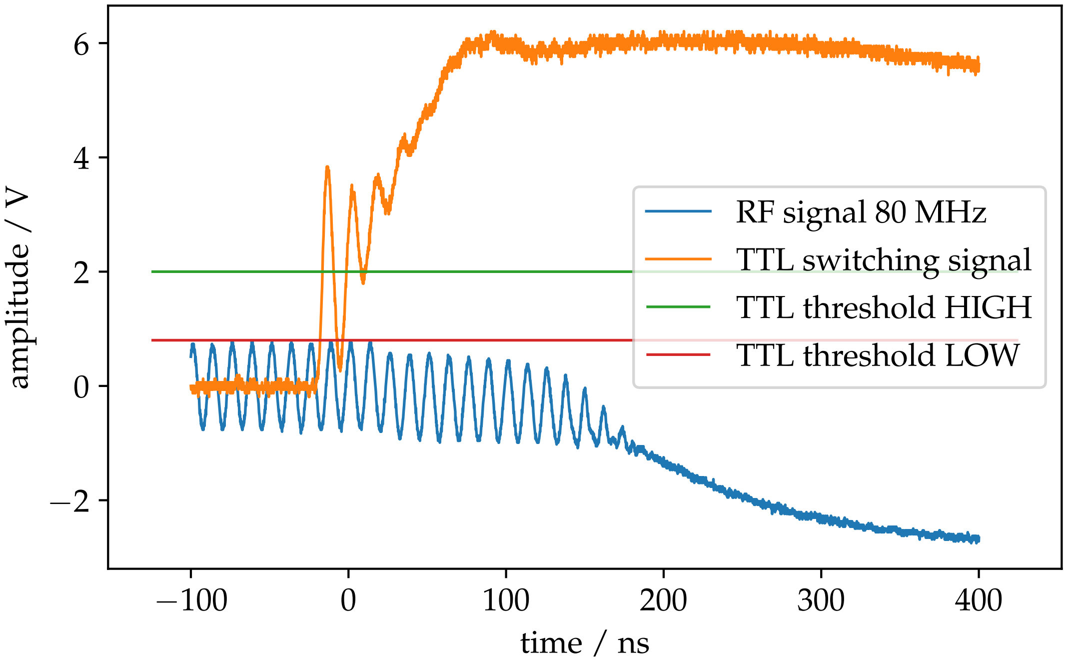

FIGURE 4.17: Result of the test measurement to determine the delay between the trigger signal and the actual shut off. The RF switch is used in combination with a TTL control box to switch off an 80 MHz RF test signal. At $t = 0$ the TTL signal exceeds the threshold for the recognition of a logic HIGH meaning that at this moment the signal is switched from ON to OFF. It takes approximately 175 ns until the RF signal has turned off. Thus, the switch is fast enough to be used for the ring-down spectroscopy.

which means that the switch now interrupts the RF signal. It can be estimated that the RF signal is switched off after 175 ns meaning that the switch is fast enough for the planned purpose.

Since environmental parameters can influence the transmission strength as well as the light coupling into the cavity does, repeating the ring-down measurement several times results in different decay curves as it is depicted in Figure 4.18a. Especially the varying intensity of the transmission signal influences the final accuracy of the determination of the finesse. It becomes obvious that the curves do not represent an ideal exponential decay. This can have different reasons. When the transmission signal becomes very weak with time, the background noise predominates. In the beginning the laser might be still stable enough to stay almost locked for a short time before the actual decay begins. Since we are interested in the photons' lifetime, one can determine it from the slope of the exponential decay function when depicting the amplitude on a logarithmic scale as it was done for Figure 4.18b. It can be recognized that one finds the best accordance with a linear slope for the curves with the highest signal amplitude, therefore this curve is taken into account for the estimation of the finesse. Figure 4.19a and Figure 4.19b show in detail the procedure to determine lifetime and finesse again in linear as

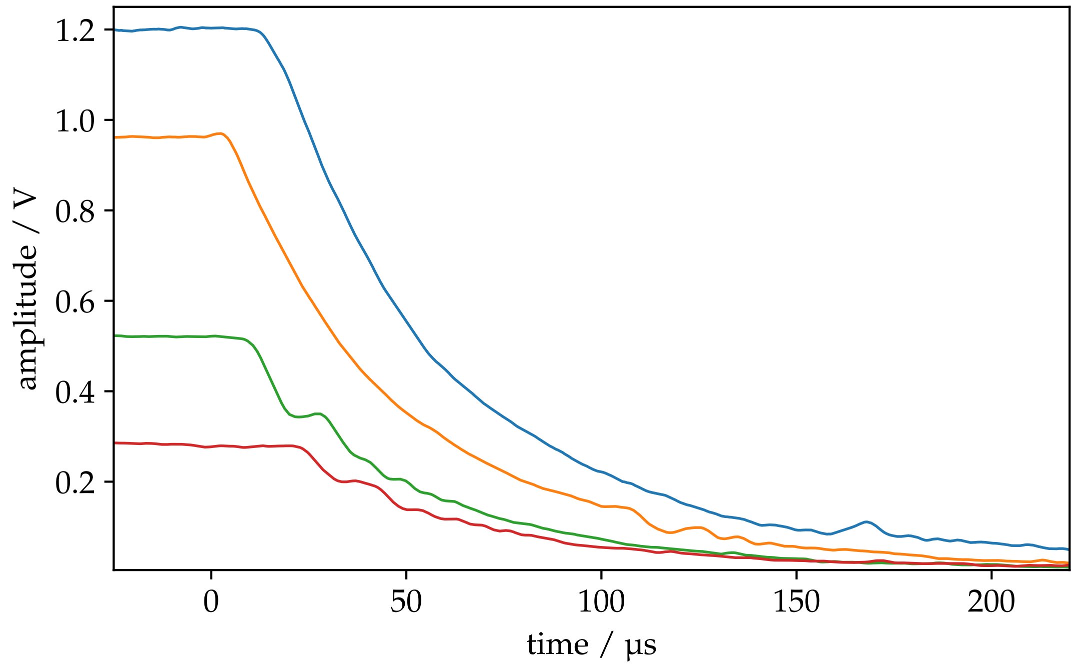

(A) linear scaling

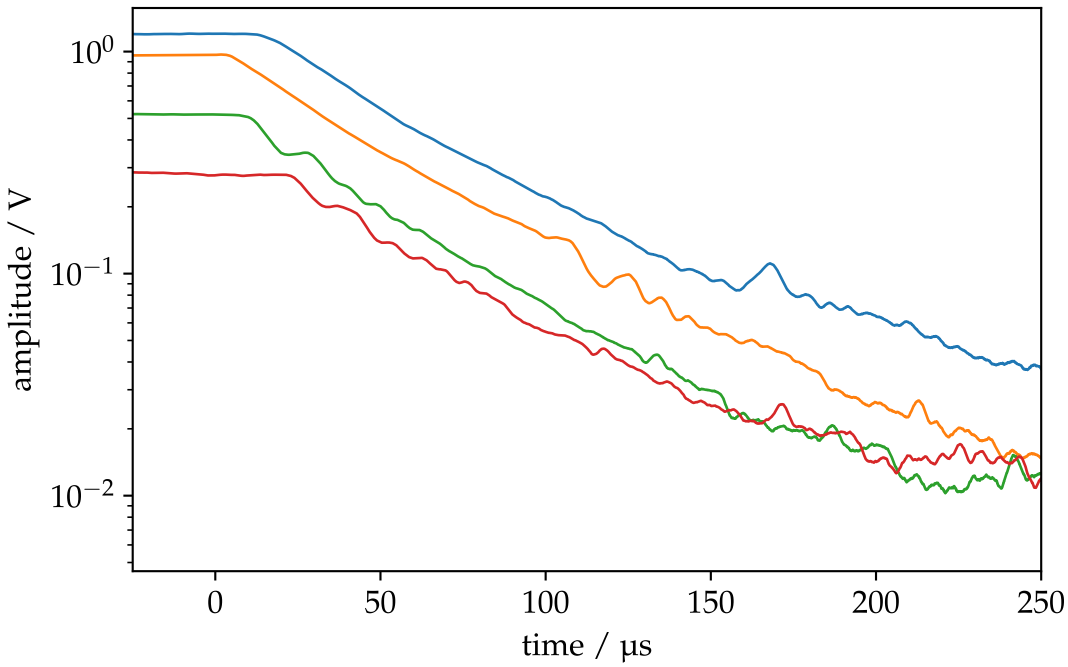

(B) logarithmic scaling. Areas with a linear slope correspond to the exponential decay of the photon population in the cavity

FIGURE 4.18: Overview of some ring-down measurements in linear and logarithmic depiction. Note that the amplitude of the transmission signal does not only depend on the current environmental parameters but also on the coupling into the cavity and the temperature inside it. The curves with the higher amplitude better represent the exponential decay.

well as in logarithmic depiction. An exponential decay function

$$f(t) = a \exp\left(-\frac{t}{\tau}\right) \tag{4.4}$$

is fit twice to the experimental data to make an estimation of the lifetime τ. In one case, a and τ are used as fit parameters while for the second fit the decay time is fixed to 44 µs with regard to the expected value from the acceptance report and only the scaling a is varied. So, one has a direct comparison to evaluate the actual finesse. In the linear depiction (a) there is no visible difference between both fits although the values for the lifetime differ by 0.6 µs. A deviation can be observed when taking a look on the logarithmic plot (b). Here, the fit functions deviate from each other and the measured transmission signal after approximately 150 µs. Since the measured signal does not decay exponentially in this area, one has to consider the appearing noise and therefore the data are neither reliable nor relevant for the estimation of the finesse. The difference of only 0.6 µs or 1.4 % can be interpreted as the normal measurement uncertainty. Thus, it can be concluded that the ring-down measurement could verify a photon lifetime arround $\tau = 44$ µs in the cavity. For converting the lifetime into a value for the finesse, one can use equation (3.2) and the relation $\tau = \frac{1}{2\pi\,\Delta\nu}$ to find

$$\mathcal{F} = 2\pi\,\nu_{\mathrm{FSR}}\,\tau\,. \tag{4.5}$$

The free spectral range of this cavity is quoted in the acceptance report with 1.5 GHz [29]. Thus, the lifetime of 44 µs corresponds to a very high finesse of approximately $\mathcal{F} \approx 410000$.

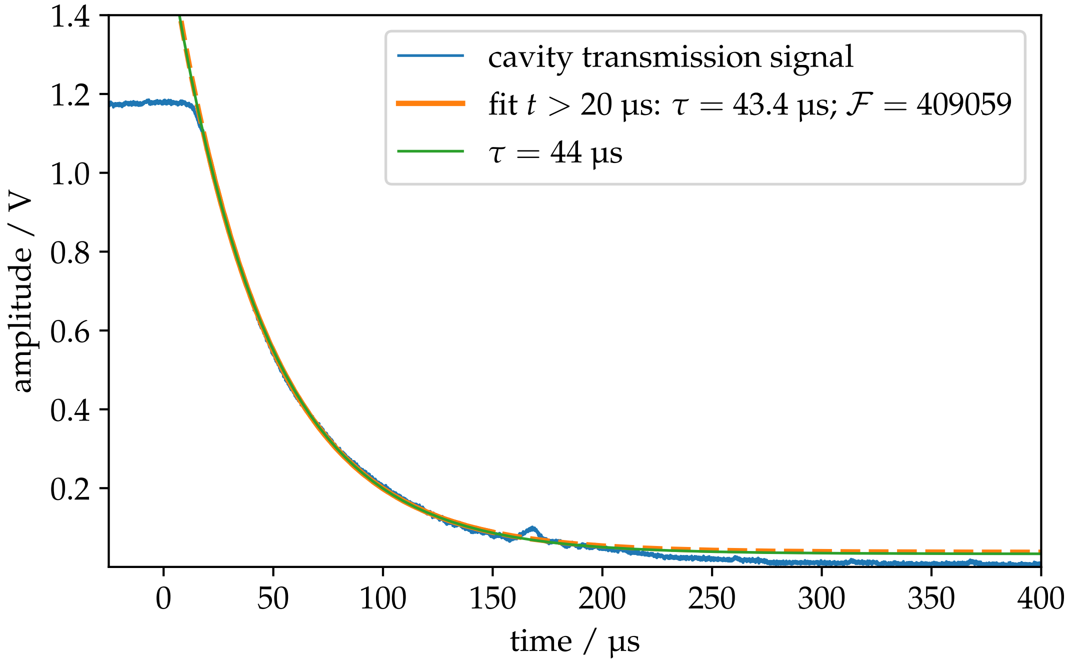

(A) linear scaling

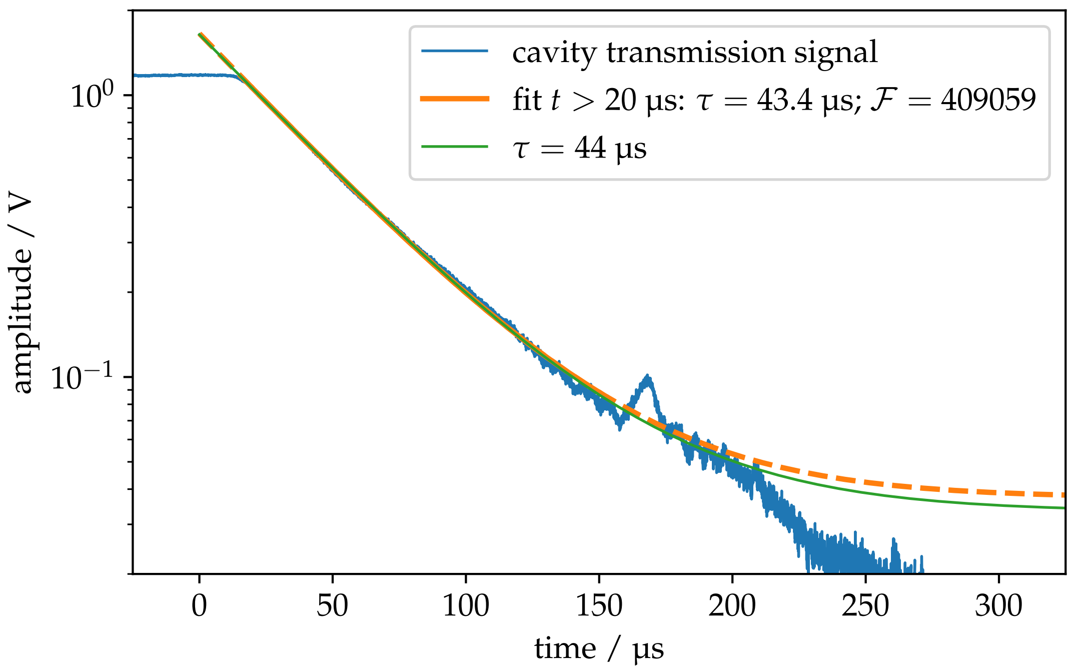

(B) logarithmic scaling

FIGURE 4.19: Ring-down cavity transmission signal and fit function to determine the photons' lifetime and finesse in comparison to the expected photon lifetime of $\tau = 44$ µs. The orange fit function adapts a as well as τ from (4.4) to find the photon's lifetime. The green fit function can be used as a reference how the decay would look if the lifetime is in accordance with the given value of 44 µs from the acceptance report.

5 Summary & Outlook

In this thesis, the *Toptica TA pro* unit together with the furhter components forming the 1001 nm laser system were systematically characterized. The aim was to investigate all relevant properties in preparation for the future usage of the laser in the Dysprosium experiment. This thesis can be understood as a detailed guide that explains how to control the laser system but also points out its ability and limits. This contains the verification of several crucial parameters quoted by the manufacturer.

The very first part was to build a basic optics setup that enables for example switching or frequency and intensity modulation of the laser light but also monitoring the wavelength and power. This is the starting point for any application either of experimental purpose or for the characterization measurements.
So far, there is still s critical point regarding this setup. The efficiency of the used AOM is with only 36 % below the typically reachable values. Together with a slight beam profile deformation due to the AOM diffraction, this leads to a relatively high power loss when it comes to coupling the light into a single-mode fiber. However, this should be easily solvable by replacing the AOM with one that is optimized for the 1001 nm wavelength.
The Tapered Amplifier compensates the limited power of a diode laser and ensures that the laser system provides a much larger output power around 2 W. By adjusting TA current and TA temperature it was possible to increase the laser power at maximum up to 1.4 W what is still below the value of 2.5 W measured at factory. An optimum can be reached when setting the temperature around 18 °C and the current nearby its upper limit of 6.2 A. The diode current should be fixed to a value around 156 mA corresponding to a seed power of approximately 50 mW that is necessary for the proper seeding of the TA. Meanwhile, a non-linear but periodically jumping increase of power was observed accompanied by a drift of the power over time. This behavior is likely in an a causal relationship with the coupling into the TA-chip. By improving the coupling, we expect to increase the power to the given factory value.
Setting the wavelength precisely to the value where we expect the desired transition is another crucial aspect. For coarse tuning it is recommended to use the diode temperature that has the largest impact on the wavelength and can change it by $2.9(1) \times 10^{-2}\,\mathrm{nm}/^{\circ}\mathrm{C}$ but needs a few minutes to settle. The piezo voltage is suitable for fast and fine tuning with $-5.5(3) \times 10^{-4}\,\mathrm{nm/V}$. The diode current has an impact of$1.8(1) \times 10^{-4}\,\mathrm{nm/mA}$ on the wavelength

but should not be used for this aim because it is required not to change, otherwise the TA might be seeded insufficiently. If the laser is not locked to the ULE cavity, the wavelength can change in average by 8.4×10^{-5} nm per hour. There seems to be a strong correlation between air pressure and wavelength drift. In contrast, the locked laser is very stable. Here, a drift was not detectable concerning the resolution of 20 MHz of the used wavemeter.
Finally, the ultra-narrow linewidth and the high finesse of the laser system were objects of this work. Using the delayed self-heterodyne linewidth measurement method, it was possible to prove the linewidth to be smaller than 10 Hz as claimed by the manufacturer. Even the free running laser has a relatively narrow linewidth around 50 kHz. The ultra-narrow linewidth is a consequence of the locking to the high finesse ULE cavity. An adapted version of the cavity ring-down spectroscopy technique was implemented to verify the finesse by determining the photons' lifetime. The measurement confirmed the estimated value of $\tau = 44\,\mu s$ that is equivalent to a finesse of $\mathcal{F} \approx 410000$.

Taking into account all the discussed properties, it can be established that the very narrow linewidth laser system at 1001 nm is well-suitable for high-precision experiments including the addressing of the 1001 nm transition in Dysprosium. After realizing the mentioned improvements for an enhanced stability, the laser system can by finally integrated to the UV lattice for the quantum gas microscope experiment.

A Beam Profile

This appendix chapter contains images of the beam profile at several positions along the optical path referring to Figure 4.1 taken with the *DataRay* beam profiler camera.[1] Figure A.1 shows as an example the beam profile of the laser light directly after the fiber and the outcoupler. Apart from the color-coded intensity pattern a cut through this plane in horizontal and vertical direction reveals an intensity profile that can be compared with a Gaussian function (4.3) to determine the beam diameter and its ellipticity. Figure A.2 gives an overview over the additional beam profiler images.

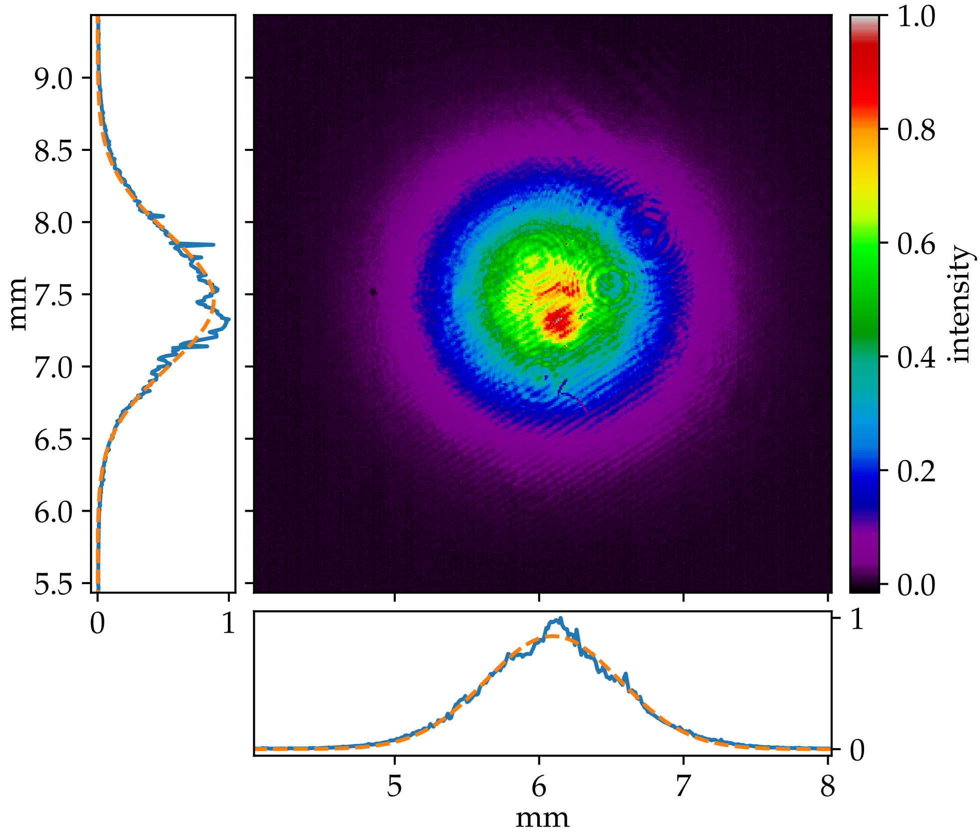

FIGURE A.1: Beam profiler camera image taken directly after the outcoupler. 2D intensity color-map accompanied by the intensity profile in x and y-direction compared to a Gaussian fit function (4.3).

[1]The beam profiler was set to a resolution of 1024×1024 pixels with an edge length of $11\,\mu m$ per pixel, so it has an active area of $11.3\,mm \times 11.3\,mm$.

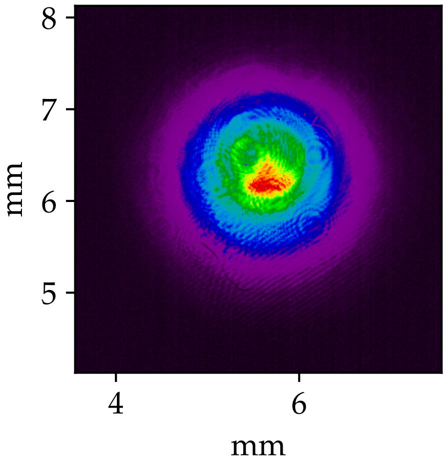

(A) Beam profile after polarizing beam splitter

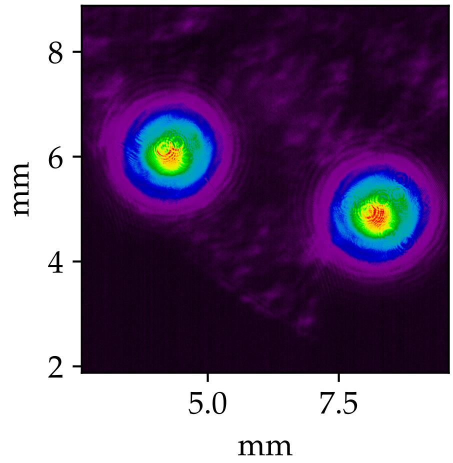

(B) Beams reflected by the beamsampler

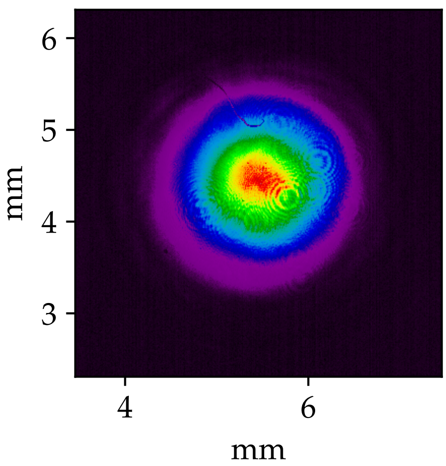

(C) Beam profile before collimator and fiber to wavemeter

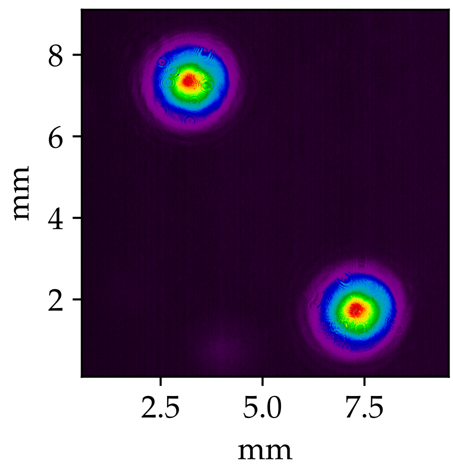

(D) Beam profile on the path going to the powermeter

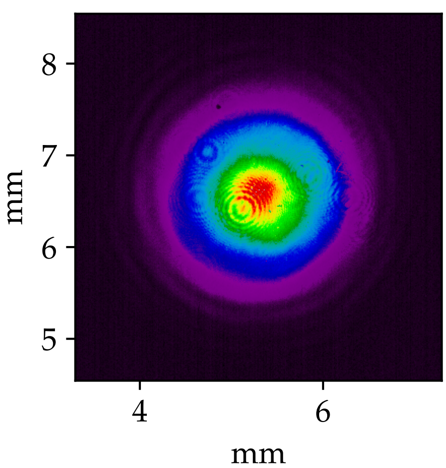

(E) Beam profile before the telescope

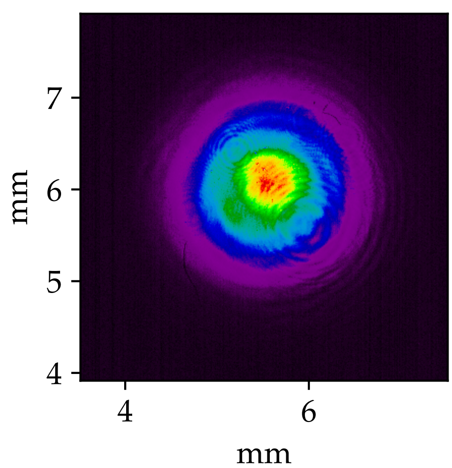

(F) Beam profile after the telescope at disabled AOM

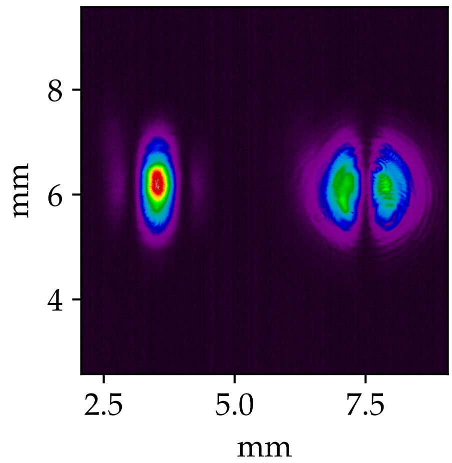

(G) Profile of diffracted beams after telescope at working AOM

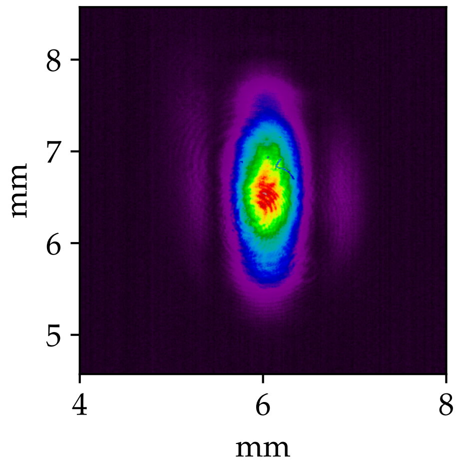

(H) Beam profile after second polarizing beam splitter

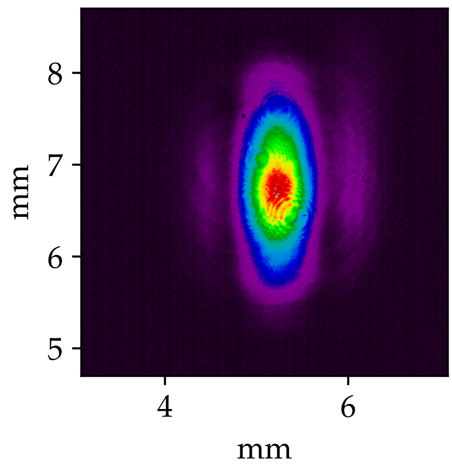

(I) Beam profile before last $\lambda/2$ waveplate

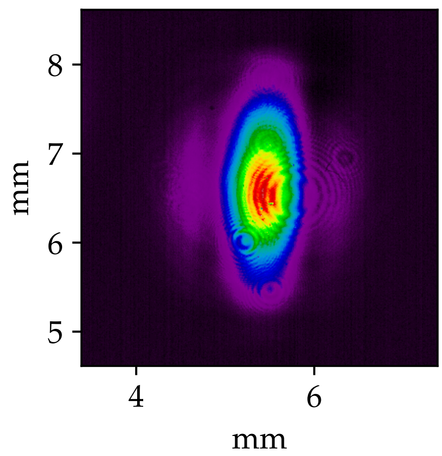

(J) Beam profile before fiber outcoupler to the experiment

FIGURE A.2: Overview of the taken beam profile images at different spots referring to Figure 4.1

Bibliography

[1] Waseem S. Bakr et al. "A quantum gas microscope for detecting single atoms in a Hubbard-regime optical lattice". In: *Nature* 462.7269 (2009), pp. 74–77. DOI: 10.1038/nature08482. eprint: 19890326.

[2] Jonathan Balewski. "Hochauflösende Photoassoziationsspektroskopie von Rydberg-Dimeren und Trimeren". 5. Physikalisches Institut. Diplomarbeit. Stuttgart: Universität Stuttgart, 2009. URL: https://www.pi5.uni-stuttgart.de/documents/abgeschlossene-arbeiten/2009-Balewski-Jonathan-Hochaufloesende-Photoassoziationsspektroskopie-von-Rydberg-Dimeren-und-Trimeren-Diplom.pdf (visited on 08/16/2023).

[3] Michael Berglund and Michael E. Wieser. "Isotopic compositions of the elements 2009 (IUPAC Technical Report)". In: *Pure and Applied Chemistry* 83.2 (2011), pp. 397–410. ISSN: 0033-4545. DOI: 10.1351/PAC-REP-10-06-02.

[4] Eric D. Black. "An introduction to Pound–Drever–Hall laser frequency stabilization". In: *American Journal of Physics* 69.1 (2001), pp. 79–87. ISSN: 0002-9505. DOI: 10.1119/1.1286663.

[5] Fabian Böttcher et al. "Transient Supersolid Properties in an Array of Dipolar Quantum Droplets". In: *Physical Review X* 9.1 (2019). DOI: 10.1103/PhysRevX.9.011051.

[6] Jamie A. Boyd and Thierry Lahaye. *A basic introduction to ultrastable optical cavities for laser stabilization*. 10 pages, 8 figures, tutorial article to appear in Am. J . Phys. 2023. URL: http://arxiv.org/pdf/2308.08015v1.

[7] Mingjun Chi et al. "Tunable high-power narrow-linewidth semiconductor laser based on an external-cavity tapered amplifier". In: *Optics express* 13.26 (2005). Journal Article, pp. 10589–10596. DOI: 10.1364/opex.13.010589. eprint: 19503273.

[8] Crystal Technology Inc., ed. *AOMO 3110-125 specifications*. archived on 03/12/2006. URL: https://web.archive.org/web/20060312022137/http://www.crystaltechnology.com/97-01672-03rD%20AOMO.pdf (visited on 08/17/2023).

[9] A. Cygan et al. "Pound-Drever-Hall-locked, frequency-stabilized cavity ring-down spectrometer". In: *The Review of scientific instruments* 82.6 (2011). Journal Article, p. 063107. DOI: 10.1063/1.3595680. eprint: 21721674.

[10] Michael C. Darrow. "Finesse Measurement in Fabry-Perot Interferometers". In: *Macalester Journal of Physics and Astronomy* 2.1 (2014). URL: https://digitalcommons.macalester.edu/cgi/viewcontent.cgi?article=1026&context=mjpa (visited on 08/30/2023).

[11] Data Ray Inc., ed. *WinCamD-LCM. 1" CMOS Beam Profiling Camera Datasheet*. URL: https://dataray-web.s3.amazonaws.com/pdf/dataray-wincamd-lcm-datasheet.pdf (visited on 08/16/2023).

[12] Christian Gross and Waseem S. Bakr. "Quantum gas microscopy for single atom and spin detection". In: *Nature Physics* 17.12 (2021). PII: 1370, pp. 1316–1323. ISSN: 1745-2473. DOI: 10.1038/s41567-021-01370-5.

[13] HighFinesse GmbH, ed. *Wavelength Meter WS6-600 Series Technical Data*. URL: https://www.highfinesse.com/en/wavelengthmeter/wavelengthmeter-further-information/technical-information-wavelengthmeter-ws6-600-series.pdf (visited on 08/23/2023).

[14] Peter Horak and Wei H. Loh. "On the delayed self-heterodyne interferometric technique for determining the linewidth of fiber lasers". eng. In: *Optics express* 14.9 (2006). Journal Article, pp. 3923–3928. DOI: 10.1364/oe.14.003923. eprint: 19516539.

[15] Shihong Huang et al. "Precise measurement of ultra-narrow laser linewidths using the strong coherent envelope". In: *Scientific reports* 7 (2017), p. 41988. DOI: 10.1038/srep41988. eprint: 28181506.

[16] Isomet Corp., ed. *Acousto-Optic Modulation Application Note*. URL: https://isomet.com/App-Manual_pdf/AO%20Modulation.pdf (visited on 08/18/2023).

[17] j-fiber GmbH Jena, ed. *Singlemode Optical Fiber 09/125*. archived on 2012-11-26. 2004. URL: https://web.archive.org/web/20121126122735/http://www.j-fiber.com/en/152/download/1150/110301084855_DB-FS-001-00-0604(09-125)1.pdf (visited on 08/25/2023).

[18] Jayampathi C. B. Kangara et al. "Design and construction of cost-effective tapered amplifier systems for laser cooling and trapping experiments". In: *American Journal of Physics* 82.8 (2014), pp. 805–817. ISSN: 0002-9505. DOI: 10.1119/1.4867376.

[19] Alexander Kramida and Yuri Ralchenko. *NIST Atomic Spectra Database, NIST Standard Reference Database 78*. eng. 1999. DOI: 10.18434/T4W30F.

[20] Thomas Maier. "Interactions in a Quantum Gas of Dysprosium Atoms". 5. Physikalisches Institut. Doktorarbeit. Universität Stuttgart, 2015.

[21] Lena Maske. "Spektroskopie des 1001 nm Übergangs von Dysprosium". Institut für Physik. Masterarbeit. Mainz: Johannes Gutenberg-Universität, 2018. URL: https://www.qoqi.physik.uni-mainz.de/files/2019/03/MA_2018_Lena_Maske.pdf (visited on 08/16/2023).

[22] L. B. Mercer. "1/f frequency noise effects on self-heterodyne linewidth measurements". In: *Journal of Lightwave Technology* 9.4 (1991), pp. 485–493. ISSN: 07338724. DOI: 10.1109/50.76663.

[23] Yu Peng. "A Novel Scheme for Hundred-Hertz Linewidth Measurements with the Self-Heterodyne Method". In: *Chinese Physics Letters* 30.8 (2013), p. 084208. ISSN: 0256-307X. DOI: 10.1088/0256-307X/30/8/084208.

[24] Niels Petersen, Marcel Trümper, and Patrick Windpassinger. "Spectroscopy of the 1001 nm transition in atomic dysprosium". In: *Physical*

Review A 101.4 (2020). ISSN: 2469-9926. DOI: 10.1103/PhysRevA.101.042502. URL: http://arxiv.org/pdf/1907.05754v2.

[25] L. Richter et al. “Linewidth determination from self-heterodyne measurements with subcoherence delay times”. In: *IEEE Journal of Quantum Electronics* 22.11 (1986), pp. 2070–2074. ISSN: 0018-9197. DOI: 10.1109/JQE.1986.1072909.

[26] Jan-Nicklas Schmidt. “Density Fluctuations in a Dipolar Quantum Gas. from Superfluids to Supersolids”. 5. Physikalisches Institut. Doktorarbeit. Universität Stuttgart, 2021.

[27] Toptica Photonics AG. “Cavity Accaptance Report”. Oct. 6, 2020.

[28] Toptica Photonics AG, ed. *FiberDock. Compact Fiber Coupler Manual*. 2015. URL: https://www.toptica.com/fileadmin/Editors_English/03_products/11_Isolators_Photonicals/02_photonicals/toptica_FiberDock_Manual.pdf (visited on 08/16/2023).

[29] Toptica Photonics AG. “TA pro Acceptance Report”. Dec. 13, 2019.

[30] D. Voigt et al. “Characterization of a high-power tapered semiconductor amplifier system”. In: *Appl. Phys. B* 72 (2001). URL: http://arxiv.org/pdf/physics/0004043v1.

[31] Yihan Xiong. “Design and characteristics of a tapered amplifier diode system by seeding with continuous-wave and mode-locked external cavity diode laser”. In: *Optical Engineering* 45.12 (2006), p. 124205. ISSN: 0091-3286. DOI: 10.1117/1.2404925.

[32] Zhongan Zhao et al. “Narrow laser-linewidth measurement using short delay self-heterodyne interferometry”. eng. In: *Optics express* 30.17 (2022). Journal Article, pp. 30600–30610. DOI: 10.1364/OE.455028. eprint: 36242160.